NUREG/CR-0550
HEDL-TME 78-7

LWR PRESSURE VESSEL IRRADIATION SURVEILLANCE DOSIMETRY

Quarterly Progress Report
April - June 1978

G. L. Guthrie
E. P. Lippincott
W. N. McElroy
R. Gold

Hanford Engineering Development Laboratory

515 177

Prepared for
U. S. Nuclear Regulatory Commission

Available from
National Technical Information Service
Springfield, Virginia 22161

NUREG/CR-0550
HEDL-TME 78-7
R5

LWR PRESSURE VESSEL IRRADIATION SURVEILLANCE DOSIMETRY

Quarterly Progress Report
April - June 1978

Prepared by

G. L. Guthrie
E. P. Lippincott
W. N. McElroy
R. Gold

Hanford Engineering Development Laboratory
P.O. Box 1970
Richland, WA 99352

Manuscript Completed: April 1979
Date Published: June 1979

Prepared for
Division of Reactor Safety Research
Office of Nuclear Regulatory Research
U. S. Nuclear Regulatory Commission
Washington, D.C. 20555
NRC FIN No. B5988-7

NUREG/CR-0550
HEDL-TME 78-7
R5

LWR PRESSURE VESSEL IRRADIATION SURVEILLANCE DOSIMETRY QUARTERLY PROGRESS REPORT JANUARY - MARCH 1978

Preparation Coordinated by G. L. Guthrie, W. N. McElroy, E. P. Lippincott, and R. Gold
Hanford Engineering Development Laboratory

ABSTRACT

This report was compiled at the Hanford Engineering Development Laboratory operated by Westinghouse Hanford Company a subsidiary of Westinghouse Electric Corporation, for the United States Department of Energy, Nuclear Regulatory Commission, under DOE contract number EY-76-C-14-2170 and NRC service request number TV-0176. It describes progress made in the Light Water Reactor Pressure Vessel Irradiation Surveillance Dosimetry Program during the reporting period.

ACKNOWLEDGEMENTS

The following organizations are presently participating in the Light Water Reactor Pressure Vessel Irradiation Surveillance Dosimetry Program and will periodically contribute to this report.

Atomic Energy Research Establishment, Harwell, England (AERE-H)

California State University Northridge (CSO-N)

Centre d' Etude de l' Energie Nucleaire - Studiecentrum voor Kern Energie (CEN/SCK), Mol, Belgium

Electric Power Research Institute (EPRI)

Fracture Control Corporation (FCC)

General Electric Vallecitos Nuclear Center (GE-VNC)

Hanford Engineering Development Laboratory (HEDL)

IRT Corporation (IRT)

Kernforschungsanlage Julich Gmbh, Germany (KFA)

Macalester College (MC)

National Bureau of Standards (NBS)

Oak Ridge National Laboratory (ORNL)

Pacific Northwest Laboratories (PNL)

Radiation Research Associates (RRA)

Rockwell International Energy Systems Group (RIES)

Rolls-Royce and Associates Limited, Derby, England (RRAL)

Science Applications Incorporated (SAI)

University of California, Santa Barbara (USCB)

University of Tennessee (UT)

Westinghouse Electric Corporation - PWR Systems Division (WEC-PWR-SD)

Westinghouse Electric Corporation - Research Division (WEC-RD)

FOREWORD

The light water reactor pressure vessel (LWR-PV) surveillance dosimetry program has been established by NRC in recognition of the importance of improving, maintaining, and standardizing neutron dosimetry, damage correlation, and the associated reactor analysis procedures used for predicting the integrated effect of neutron exposure to LWR pressure vessels. A vigorous research effort attacking the same measurement and analysis problems goes forward worldwide, and strong cooperative links between the NRC supported activities at HEDL, ORNL, and NBS and those supported by CEN/SCK (Mol, Belgium), EPRI (Palo Alto, USA), KFA (Jülich, Germany) and several U. K. laboratories have been established The major benefit of this program will be a significant improvement in the accuracy of the assessment of the remaining safe operating lifetime of light water reactor pressure vessel.

The primary objective of the multi-laboratory program is to prepare an updated and improved set of dosimetry, damage correlation, and associated reactor analysis ASTM Standards for LWR-PV irradiation surveillance programs. Supporting this objective are a series of analytical and experimental validation and calibration studies in "Standard, Reference, and Controlled Environment Benchmark Fields," reactor "Test Regions," and operating power reactor "Surveillance Positions."

These studies will establish and certify the precision and accuracy of the measurement and predictive methods which are recommended for use in the ASTM Standards. Consistent and accurate measurement and data analysis techniques and methods, therefore, will have been developed and validated along with guidelines for required neutron field calculations that are used to correlate changes in material properties with the characteristics of the neutron radiation field. It is expected that the application of the established ASTM Standards will permit the reporting of measured materials property changes and neutron exposures to an accuracy and precision within bounds of 10 to 30%, depending on the measured metallurgical variable and neutron environment.

The assessment of the radiation-induced degradation of material properties in a power reactor pressure vessel requires accurate definition of the neutron field from the outer region of the reactor core to the outer boundaries of the pressure vessel. Problems with measuring neutron flux and spectrum are associated with two distinct components of LWR-PV irradiation surveillance procedures: (1) proper application of calculational estimates of the neutron fluence delivered to the first half-thickness of the vessel steel; and (2) understanding the relationship between pressure vessel material property changes and the metallurigcal test specimens irradiated in test reactors and at accelerated neutron flux positions in operating power reactors.

The first component requires validation and calibration experiments in a variety of neutron irradiation test facilities including LWR-PV mock-ups, power reactor surveillance positions, and related benchmark neutron fields. The benchmarks serve as a permanent measurement reference for neutron flux and fluence detection techniques, which are continually under development and widely applied by laboratories with different levels of capability. The second component requires a serious extrapolation of an observed neutron-induced mechanical property change from test reactor "test regions" and operating power reactor "surveillance positions" to locations inside the body of the pressure vessel wall. The neutron flux at the vessel is up to one order of magnitude lower than at surveillance specimen positions and up to two orders of magnitude lower for test reactor positions. Furthermore, the neutron spectrum at the surface and within the vessel is substantially altered.

In order to meet the reactor pressure vessel radiation monitoring requirements, a variety of neutron flux and fluence detectors are employed, most of which are passive. Each detector must be validated for application to the higher flux and harder neutron spectrum of the test reactor "test region" and to the lower flux and degraded neutron spectrum at "surveillance positions". Required detectors must respond to neutrons of various energies so

that multigroup spectra can be determined with accuracy sufficient for adequate damage response estimates. Proposed detectors for the program include radiometric detectors, helium accumulation fluence monitors, and solid state track recorders.

The necessity for pressure vessel mock-up facilities for dosimetry investigations and for irradiation of metallurgical specimens was recognized early in the formation of the NRC program. Experimental studies associated with high and low flux versions of a PWR pressure vessel mock-up have begun. As specialized benchmarks, these facilities will provide well-characterized neutron environments where active and passive neutron dosimetry, various types of LWR-PV neutron field calculations, and temperature-controlled metal damage exposure are brought together.

The results of the measurement and calculational strategies outlined here will be made available for use by the nuclear industry as ASTM Standards. Federal Regulation 10CFR50 already calls for adherence to several ASTM Standards which require incorporation of flux monitors and post-irradiation evaluation in LWR-PV irradiation surveillance. Revised and new standards in preparation will be carefully structured to be up-to-date, flexible, and, above all, consistent.

CONTENTS

515 185

FIGURES

515 186

FIGURES (Cont'd)

TABLES

SUMMARY

Hanford Engineering Development Laboratory
(HEDL)

Forty continuous gamma-ray spectra were obtained from the scoping measurements made in the Poolside Critical Assembly facility at ORNL. Measurements were made at five radial distances from the PCA surface, at two different axial levels, with and without reactor power, and with two different physical configurations. The two configurations were (1) with the pressure vessel wall simulator and thermal shield both in place, and (2) with both these items removed. Preliminary gamma dose rates have been computed. The detection system and associated electronic and data acquisition systems seem adequate for gamma-ray spectrometry scoping measurements.

Solid State Track Recorders have been prepared for irradiation in the Brown's Ferry 3 (BF3) and McGuire I reactors. Developmental work is proceeding in the adaptation of electroplating techniques for production of deposits. These techniques have been used to prepare deposits of Th, U, Np, and Pu. Mass analysis of the deposits has been initiated. It has been found possible to achieve deviations from uniformity of less than five percent.

Additional work has been done in analyzing the relationship between the irradiation induced shift in nil ductility temperature and chemical composition. The embrittlement coefficients for the elements have been tabulated in terms of weight percent of the elements and additional statistical tests have been made on the statistical significance of the various coefficients.

Oak Ridge National Laboratory
(ORNL)

Design, fabrication and preparation are continuing in the preparation of the Pool Critical Assembly Pressure Vessel Wall Benchmark Facility for dosimetry experiments. Work performed this quarter included design of free-field measurement facilities, a fission chamber tube for run-to-run normalization,

core mapping rigs, and a lead thermal shield. Analyses and documentation of the adequacy of the structural capabilities of the PCA facility were completed by ORNL General Engineering.

Assembly, layout work and detailed design of the ORR experiment facility are 85% complete. The Quality Assurance Program Plan for both the PCA an PSF have been completed and approved by the management. Design support neutron transport calculations have been made to evaluate design variations involving (1) sandwiching test specimens between copper plates, and (2) placing a set of test specimens directly behind the thermal shield. These variations were found to cause acceptably small changes in the spatial and spectral characteristics of the neutron flux.

Drawings of the Instrumented Irradiation Capsule which simulates the pressure vessel wall are about 50% complete. Two dimensional heat flow models have been developed for analyses of the simulated pressure vessel wall and the surveillance specimen capsule.

Rockwell International Energy Systems Group (RIES)

Preliminary results are given for helium analyses of boron and lithium Helium Accumulation Fluence Monitors (HAFMs) irradiated in the Fission Cavity of the BR1 reactor at Mol, Belgium. The results have not yet been corrected for neutron self-shielding or flux gradients. A total of 113 HAFMs have been prepared and shipped for inclusion in irradiations to be conducted in core and reflector positions of the FRJ-1 and FRJ-2 reactors in Julich, West Germany. The results will be compared with data from HEDL and CEN/SCK dosimeters irradiated simultaneously at the same locations.

515 190

Hanford Engineering Development Laboratory (HEDL)

A. CONTINUOUS GAMMA-RAY SPECTROMETRY SCOPING MEASUREMENTS AT THE PCA

Raymond Gold
Tang Chiao
Bruce J. Kaiser

Objective

To obtain continuous gamma-ray spectral and gamma dose rate scoping measurements in the Poolside Critical Assembly (PCA) at Oak Ridge National Laboratory (ORNL).

Summary

Forty continuous gamma-ray spectra were obtained from the scoping measurements made in the Poolside Critical Assemby (PCA) facility at ORNL. These spectra were taken at five different distances from the PCA surface and at two different axial levels both with and without reactor power. Measurements were performed in two different environments:

1. In-Situ - the low power pressure vessel mockup at the PCA, including the thermal shield and pressure vessel simulator.

2. Free Field - the unperturbed water environment without the presence of the thermal shield and pressure vessel simulator.

After initial data analysis, the sources of the gamma-rays were studied and identified, and the preliminary gamma dose rates were computed. As a result of these efforts, it was determined that:

1. The detection system performed quite adequately. However, the associated cooling system must be improved in order to better maintain the required low detector temperature in the relatively hot ~39°C, PCA environment.

2. The electronic and the data acquisition systems used for gamma spectrometry were acceptable.

3. Preliminary data analysis techniques are adequate. However, results to date are only preliminary, and systematic corrections must be determined and applied to the raw data to reduce the uncertainty of the results.

Accomplishments and Status

Introduction

The radiation field of the pressure vessel of a light water reactor is complicated, consisting principally of neutrons and gamma-rays. To understand and define this complex radiation field is a major task of the LWR Pressure Vessel Irradiation Surveillance Dosimetry Program. Various methods have been developed to measure and define the neutron field to this program. In this work, Compton Recoil Gamma-Ray Spectroscopy (CGS) developed by Gold[1] has been employed for the measurement of the continuous gamma-ray component of this mixed radiation field and for determining the absolute gamma dose rates.

Measurement of this gamma-ray component is important, not only as the major radiation constituent of a reactor field, but also provides for further studies of the interdependent relationship between the neutron and the gamma-ray components of a power reactor environment. The measurement of the continuous gamma-ray spectrum is of special interest to the LWR-PV Irradiation Surveillance Dosimetry Program, because the design and the development of the Pool Side Facility (PSF) requires information regarding gamma heating. The results from these measurements will provide this needed information.

Detector, Electronic Instrumentation and Data Acquisition System

A high resolution lithium drifted silicon solid state detector [Si(Li) detector] was used in this work. Rather than the customary application of

solid state detectors, i.e., the direct detection of discrete photo-peaks, this method uses the detector response for measurement of the Compton recoil electron distribution induced by the continuous gamma-ray spectrum of interest. The Compton electron distribution and the continuous gamma-ray spectrum are related by an integral equation, based on the well known Klein-Nishina formula for Compton scattering. In terms of the measured Compton recoil electron distribution, the continuous gamma-ray spectrum can be determined with appropriate unfolding techniques.

Figure HEDL-1 displays the Si(Li) detector and vacuum chamber components. A detector of this size (1cc) can effectively measure gamma-rays from approximately 0.1 to 2.4 MeV. The detector was mounted in a stainless steel vacuum chamber which was maintained at approximately 1×10^{-5} Torr by a small on-line ion pump. The detector was cooled with a Thermo Electric Cooler (TEC) which could decrease the detector temperature to approximately $-23^{\circ}C$. Components at the end of the detector holder were made of aluminum to improve heat transfer properties within the vacuum chambers. As a result of cooling, the detector resolution was improved to better than 10 keV for electron line width (FWHM). During a measurement period, the operating detector temperature normally held at approximately $21^{\circ}C$. However, because of insufficient heat capacity of the detector in the relatively hot PCA environment ($\sim 39^{\circ}C$), the detector temperature increased after a very short time period (2 to 3 minutes). Therefore, during each run, the detector had to be withdrawn frequently for additional cooling.

A fast low-noise ORTEC 1/ A preamplifier was used in this work. As shown in Figure HEDL-2, this preamplifier had been modified so that it could be installed close to the detector probe. This requirement necessitated a cylindrical design for the preamplifier housing. Figure HEDL-3 displays the entire spectrometer consisting of detector probe, preamplifier and the on-line ion pump. Filler inserts of lucite and steel were used in the experimental tubes to simulate water and steel environments, respectively.

The electronic instrumentation system is depicted in Figure HEDL-4 in block diagram form. The signal from the ORTEC research amplifier was fed into an ORTEC 552 pulse shape analyzer. The pulse shape analyzer generates two fast negative pulses for each input signal. The time difference between the two fast negative pulses depends on the input pulse shape. Therefore, using these two negative pulses as the starting and stopping pulses of an ORTEC 467 time-to-amplitude converter (TAC), different input pulse shapes could be distinguished. Since the Si(Li) detector output pulse shape differs for Compton recoil electrons, noise pile-up, wall events, etc., with the help of this Pulse Shape Discriminator (PSD), one can discriminate against undesirable signals from the detector. Pulses of acceptable shape passed through the linear gate and were sorted by the data acquisition system.

The data acquisition system used for this work was a multi-user, multi-purpose, mini-computer-Tennecomp TP-50 system. The TP-50 system was not only used as a multi-channel analyzer, but also as a computer, performing on-line data analysis. This latter capability is essential to the adjustment of the electronic instrumentation, especially the PSD, and will be elaborated upon later in this report. Figure HEDL-5 is a picture of the TP-50 and associated peripheral equipment, which include two floppy disk units, a magtape drive, and X-Y plotter, and a line printer. The data taken by the TP-50 system can be transferred to any one of these peripherals.

Experimental Methods and Procedures

Figure HEDL-6 shows a photograph of the PCA reactor core and simulated pressure vessel assembly. The whole facility is set in a seventeen foot deep water pool. The LWR pressure vessel mockup at the PCA can be found in Figure HEDL-7. The reactor window, the experimental access tubes, and the void box were made of aluminum. The fabrication material for the pressure vessel simulator was carbon steel, and the thermal shield was made of the stainless steel. Figure HEDL-8 is a schematic view of this facility from above. The circles indicate the positions of the experimental access tubes. The distance between the reactor window and each experimental access tube is marked

on the top of this figure as W-XX. In this work, measurements were taken at five different positions, which are indicated by crosses in Figure HEDL-8. Two continuous gamma-ray spectra were taken at each of these five positions; one at the midplane and one 6.25" above the midplane. Background spectra were taken with the reactor shut down and measurements were repeated with the reactor at low power. In order to maintain acceptable counting rates, the power of the reactor was set at different levels for different positions. The counting rates for these experiments varied from 60,000 to 115,000 counts/sec, which resulted in an ADC deadtime of roughly 3-9%. All gamma dose rates obtained by analyzing these spectra were normalized to a one-watt reactor power level. The same measurements were repeated to obtain free field spectra with the Pressure Vessel Simulator, void box, and the thermoshield removed.

Before measurements were taken, it was important to set the electronic instrumentation properly, especially the PSD, so that only pulses corresponding to acceptable Compton recoil electrons are sorted by the data acquisition system. In order to do so, a ^{137}Cs source, which emits a monoenergetic gamma-ray at 0.6616 MeV, was used to give a known electron recoil distribution. One can calculate the Gaussian-broadened theoretical Compton electron distribution for this source using the well-known Klein-Nishina formula. By comparing the measured and theoretically calculated electron distributions, one can adjust the pulse shape analyzer setting until good agreement between experiment and theory is obtained. Figure HEDL-9 shows a typical comparison between the experimental and the theoretical ^{137}Cs Compton electron distribution after proper adjustment of the PSD. Once good agreement is obtained, one can be confident that a proper setting of electronic instrumentation has been achieved for the actual data collection. In the present work, the calculation of the ^{137}Cs electron distribution and comparison plots between measurement and calculation were performed by the TP-50 on-line computer. The computer code GABCO[2,3] was used for these on-line comparisons. This same calibration procedure was repeated several times in the course of the experiment to assure proper performance of the electronic instrumentation.

Data Analysis

A detailed discussion of the data analysis and computer techniques can be found in References 1 and 2. Hence, only a brief description of the basic mathematical relations between the Compton-electron distribution and the gamma-ray spectrum need be given here.

The relationship between the unfolded scalar gamma flux, $\Phi(\epsilon_o)$, and the measured Compton-electron continuum, $W_c(E)$, is given by:

$$W_c(E) = N_e \int \frac{d\sigma_c}{dE}(E, \epsilon_o)\, \Phi(\epsilon_o) d\epsilon_o \qquad (1)$$

where E and ϵ_o are the measured electron energy and the corresponding photon energy, respectively. N_e is the total number of electrons in the detector and $\frac{d\sigma_c}{dE}$ is the differential Compton-scattering cross section (per free electron). The desired differential cross section can be obtained directly from the Klein-Nishina formula in the following form:

$$\frac{d\sigma_c}{dE}(\epsilon_o, E) = \frac{\pi r_o^2}{(\epsilon_o - E)^2} \left\{ \left(\frac{E}{\epsilon_o}\right)^2 + 2\left(\frac{\epsilon_o - E}{\epsilon_o}\right)^2 + \frac{\epsilon_o - E}{\epsilon_o^3}\left[(E-1)^2 - 1\right] \right\} \qquad (2)$$

where r_o is the classical electron radius. For the purposes of data reduction, Eq. (1) is written in matrix form

$$\underline{W_c} = C\Phi \qquad (3)$$

where $\underline{W_c}$ and Φ are vector representations of the continuous electron and photon spectrum, respectively. C is the Compton matrix, which is defined in terms of the response kernel as

$$C_{ij} = N_e \int_{(\epsilon_o)_j}^{(\epsilon_o)_{j+1}} \frac{d\sigma_c}{dE} (E_{ij}\epsilon_o) d\epsilon_o, \quad i\ j = 1, 2, \ldots m \qquad (4)$$

Using Equations (3) and (4), with the help of high speed iterative computer techniques, measured electron distributions can be readily unfolded to obtain the continuous gamma-ray spectra.

In the present work, the computer code COMSCAT[2,3] was used to unfold all measured electron spectra into gamma-ray spectra. The electron spectrum taken at TSB midplane with zero reactor power is displayed in Figure HEDL-10. Figure HEDL-11 illustrates the gamma spectrum obtained by unfolding the data given in Figure HEDL-10. The sharp break observed in Figure HEDL-10 at approximately 1.35 MeV corresponds to the Ba-La transition gamma peak at 1.60 MeV, which is clearly evident in Figure HEDL-11. In the present work, all electron spectra were unfolded as outlined above without further corrections to the raw data. However, to obtain absolute gamma spectra, several systematic corrections need to be applied before unfolding. The Si(Li) detector used in this work had a sensitive volume of only 1cc. Consequently, there exists the probability that recoil electrons can escape from the sensitive region of the detector. This probability increases with increasing electron energy. This is an example of finite size effects.[1] In the future, corrections will be applied to account for finite size effects. In addition, an efficiency correction factor related to detector geometry, ADC deadtime, etc., must be determined.

Knowing the absolute continuous gamma-ray spectrum, gamma dose rates can be computed by the computer code DOSE. The detailed basis for this analysis, as well as a full description of the DOSE code, can be found in References 1 and 2.

Results and Discussion

All forty measured electron spectra and unfolded gamma spectra have been stored for future reference and are available upon request. Also stored are

computer outputs of COMSCAT and DOSE. A typical electron spectrum at the TSB midplane location at a reactor power level of 350 mW is displayed in Figure HEDL-12. The corresponding unfolded gamma-ray spectrum is shown in Figure HEDL-13. Only raw data of the Compton electron distribution was used in this analysis. Several gamma peaks are clearly identified as idicated in Figure HEDL-13. Identification of these gamma-ray peaks is based on the in-situ PCA environment. One may note the peak arising from annihilation at radiation 0.51 MeV; the Ba-La transition peak at 1.60 MeV; the peak from neutron capture by hydrogen in water at 2.23 MeV; and peaks from neutron inelastic neutron scattering in ^{27}Al, ^{56}Fe, and ^{54}Fe at 0.85, 1.0, 1.23, and 1.42 MeV. While it is the intention of this work to provide absolute measurements of gamma-ray continuum, the capability of identifying peaks of sufficient intensity above the continuum definitely indicates that:

1) the performance of detection assembly and electronic instrumentation are satisfactory.

2) the mathematical concepts and unfolding techniques used in the computer code for data analysis are appropriate. However, in order to provide absolute intensity measurements of gamma-ray continuua, corrections for finite size effects as well as other systematic effects must be applied to electron spectra in the data analysis.

Figure HEDL-14 displays the gamma dose rate as a function of the distance from the PCA window. The plot on the left of the Figure HEDL-14 gives the gamma dose rates normalized to a one watt reactor power level, whereas the right hand plot is background gamma dose rate obtained with the reactor shut down. Since these results were computed without corrections, only the relative trend of the computed dose rate as a function of the distance from the PCA window is meaningful. The slow exponential decrease of the dose rate in the water, and the much faster exponential decrease in the pressure vessel simulator, is completely consistent with expectations.

Expected Achievements in the Next Reporting Period

The cooling system for the Si(Li) detector will be improved. Corrections for finite detector size, as well as efficiency, will be determined experimentally. In addition, the electronic instrumentation will be optimized for high count rate applications.

References

1. R. Gold, "Compton-Recoil Gamma-Ray Spectroscopy," Nucl. Instr. Methods, 84, 173-194 (1970)

2. R. Gold, I. K. Olson, Analysis of Compton Continuum Measurements," ANL-7611, Argonne National Laboratory, Argonne, IL, (1970).

3. T. Chiao, R. Gold, B. J. Kaiser, "Computer Codes for Continuous Gamma-Ray Spectrometry," LWR Pressure Vessel Irradiation Surveillance Dosimetry Quarterly Progress Report--Jan.-March, 1978, HEDL-TME 78-6, Hanford Engineering Development Laboratory, Richland, WA.

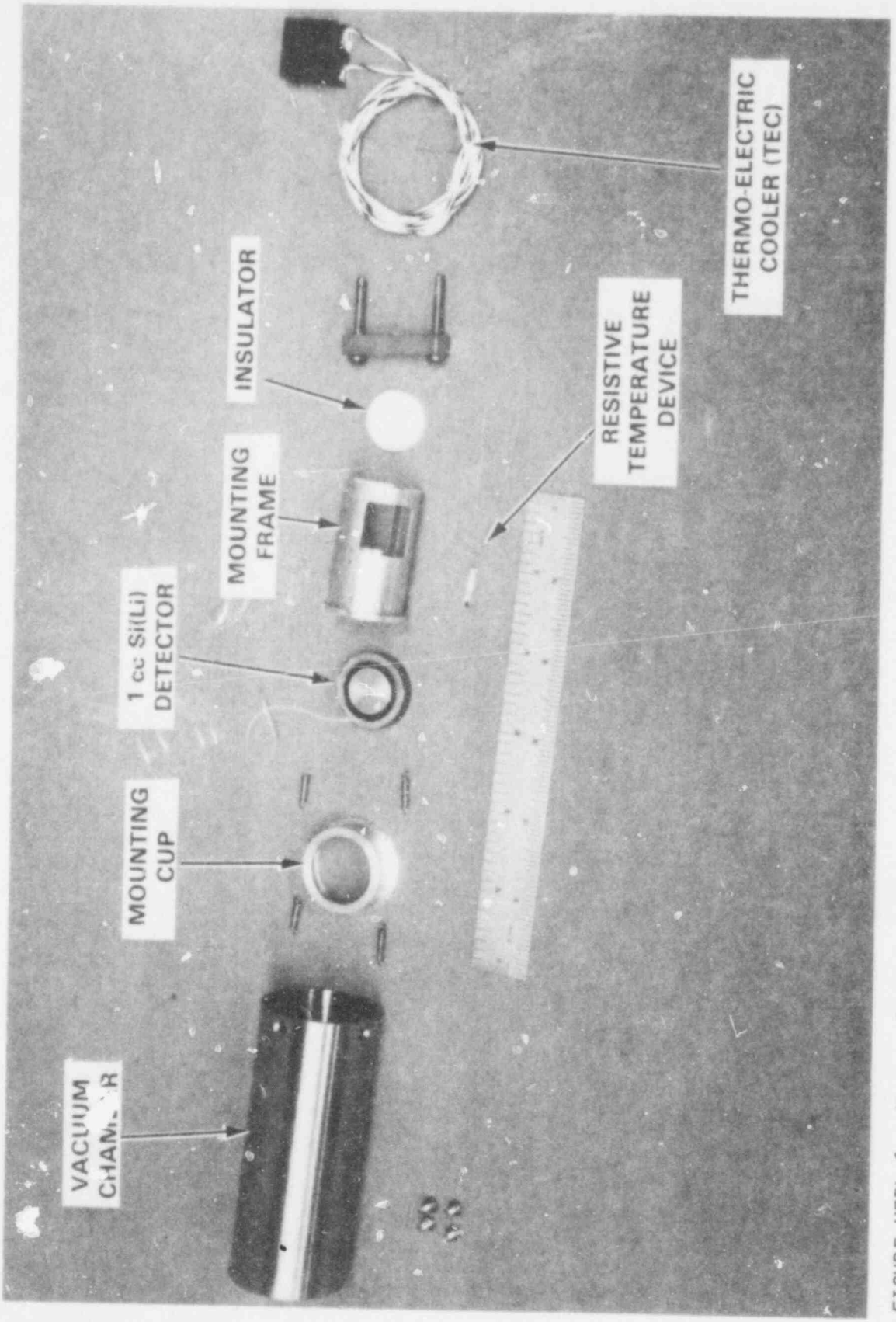

FIGURE HEDL-1. Vacuum Chamber Components for the 1cc Si(Li) Detector. Neg. 7811291-7

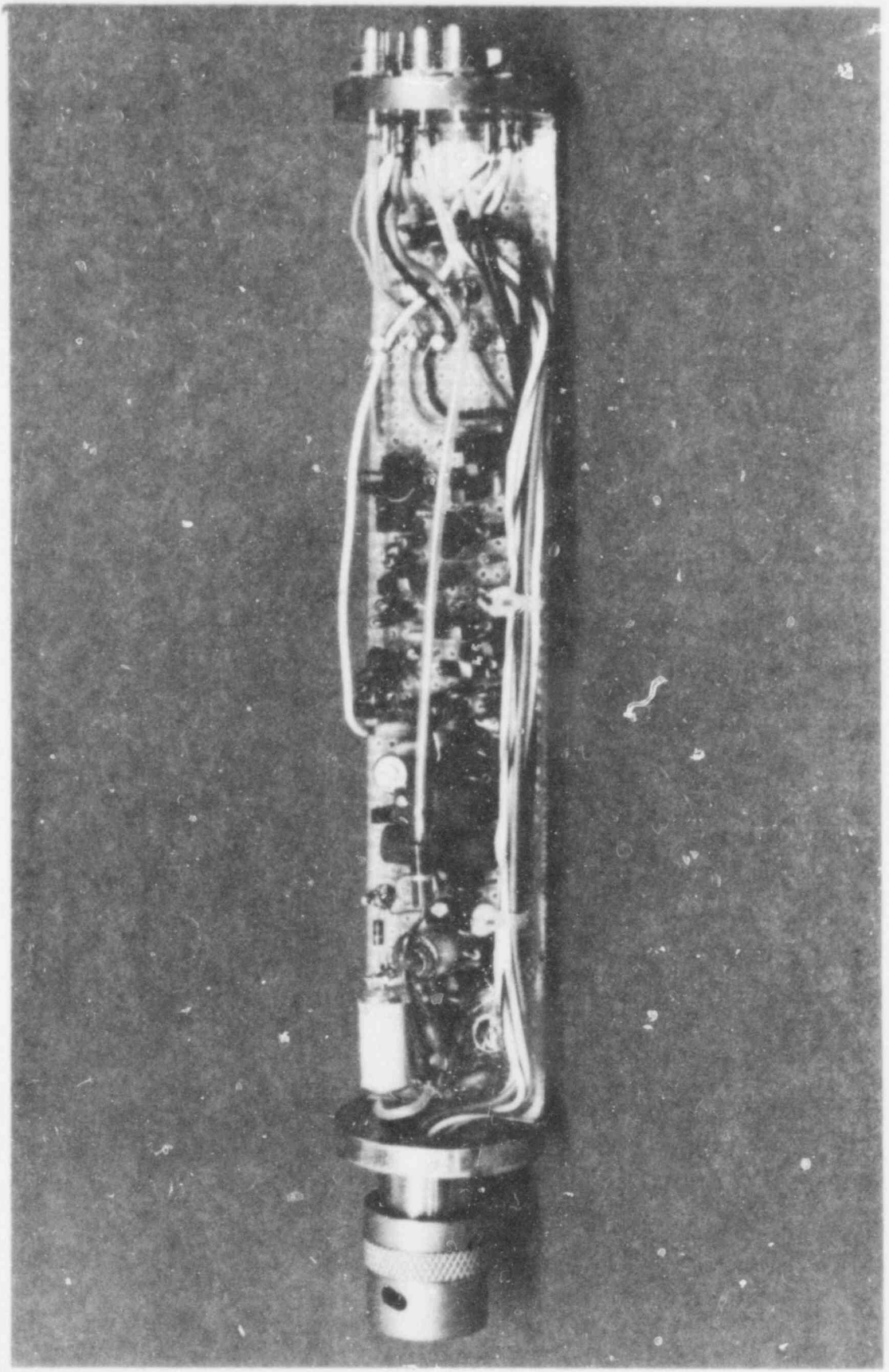

FIGURE HEDL-2. Cylindrical Layout of the ORTEC (142A Pre-Amplifier). Neg. 7801704-5 cn

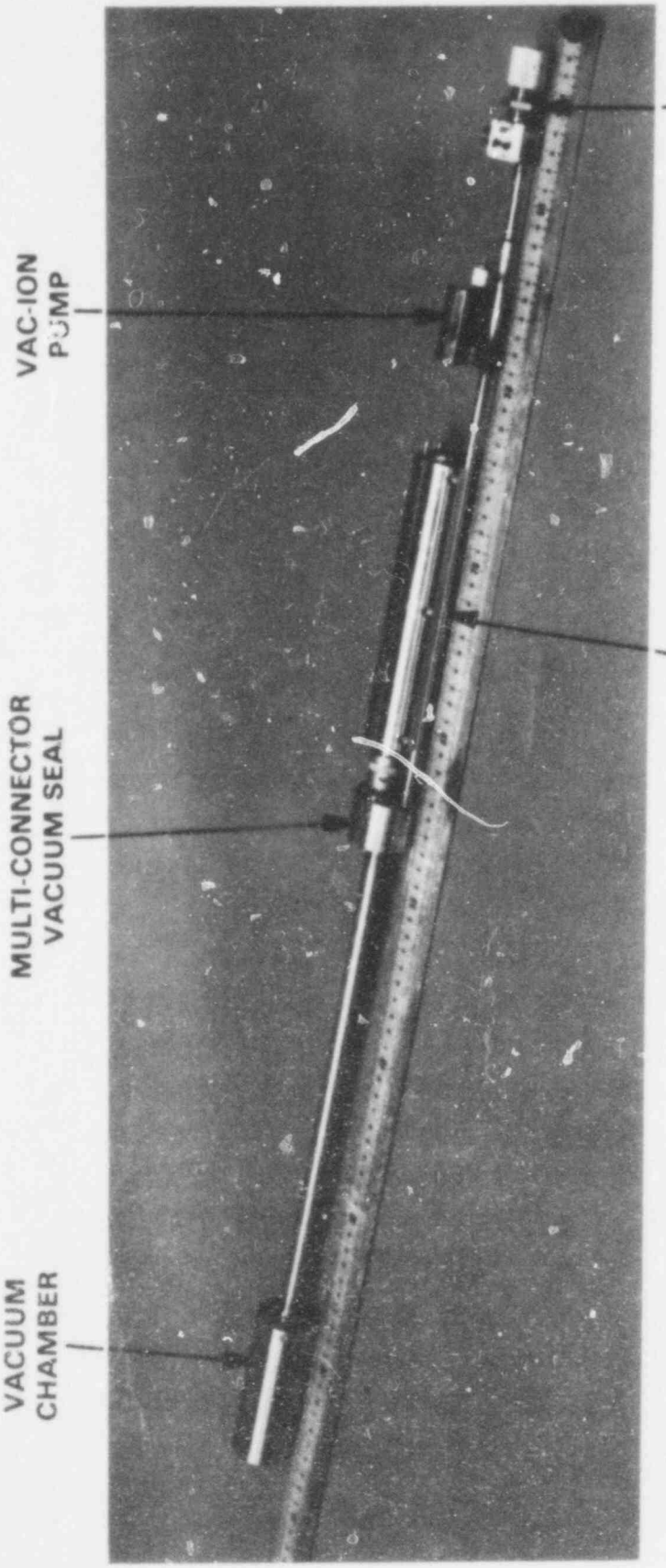

FIGURE HEDL-3. Detection Probe for Continuous Compton Gamma-Ray Spectrometry. Neg. 7811291-6

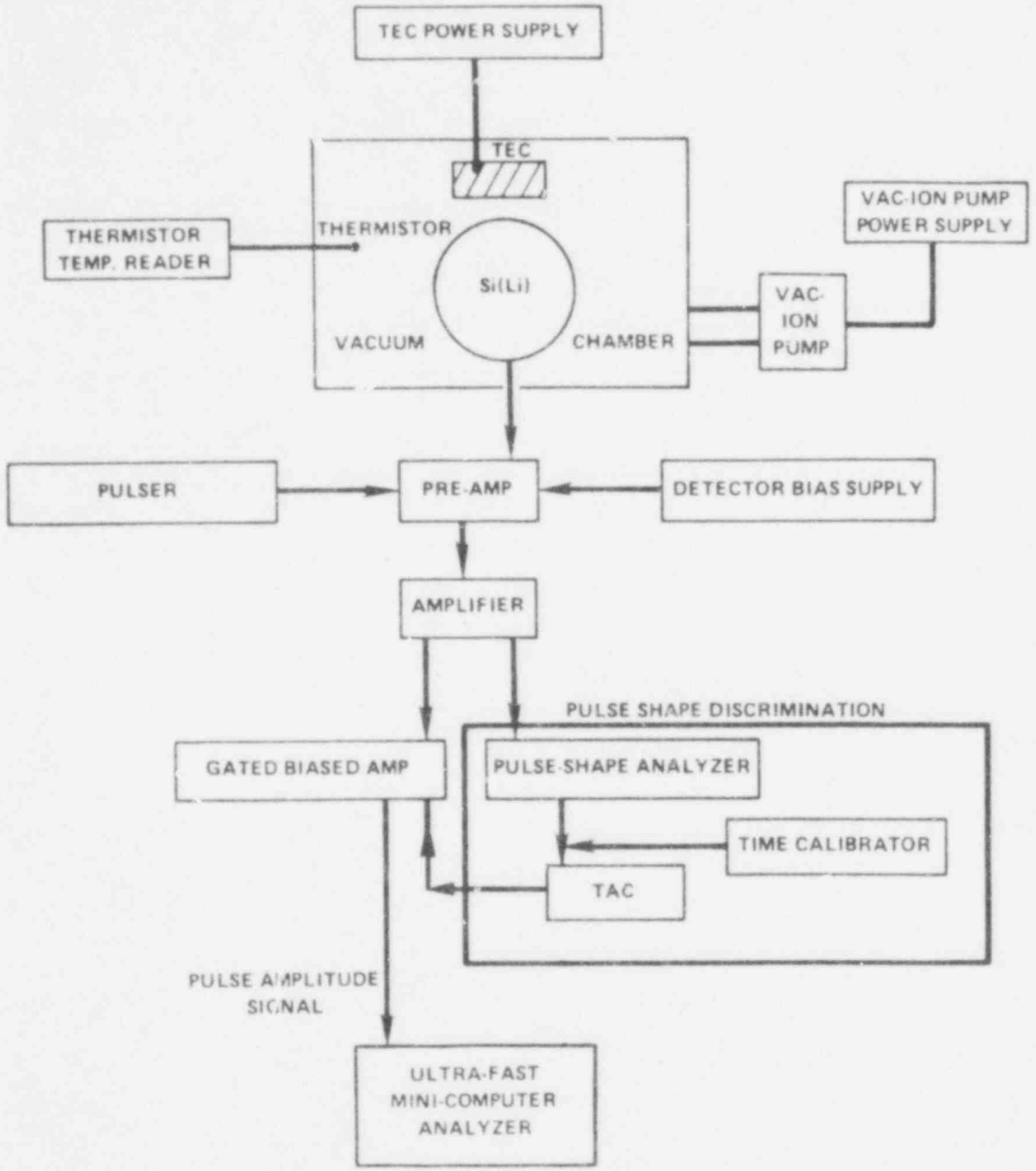

HEDL 7809-003.2

FIGURE HEDL-4 Block Diagram of Electronic Instrumentation.
Neg. 7809933-1

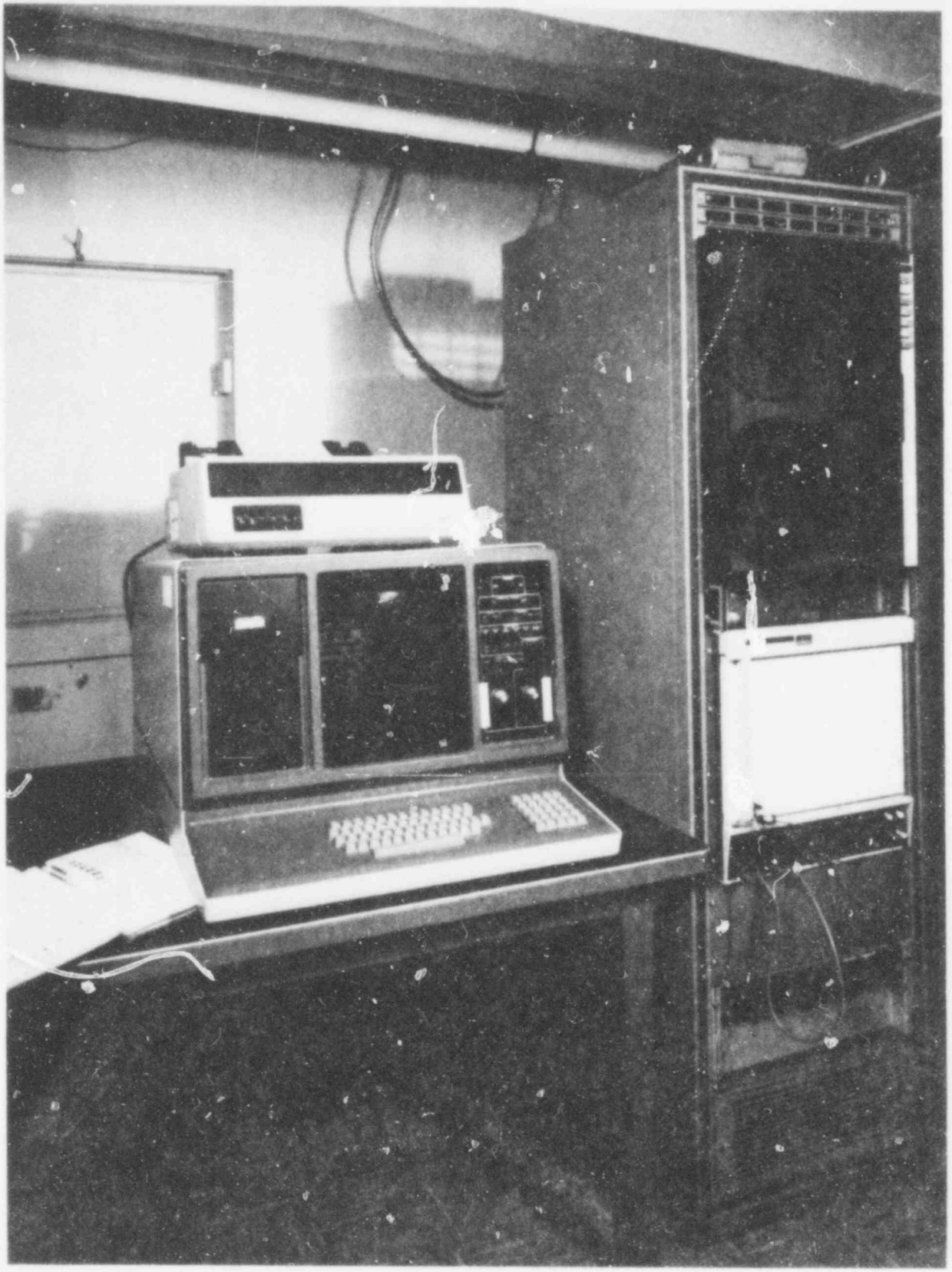

FIGURE HEDL-5. Data Acquisition System. Neg. 7811291-9

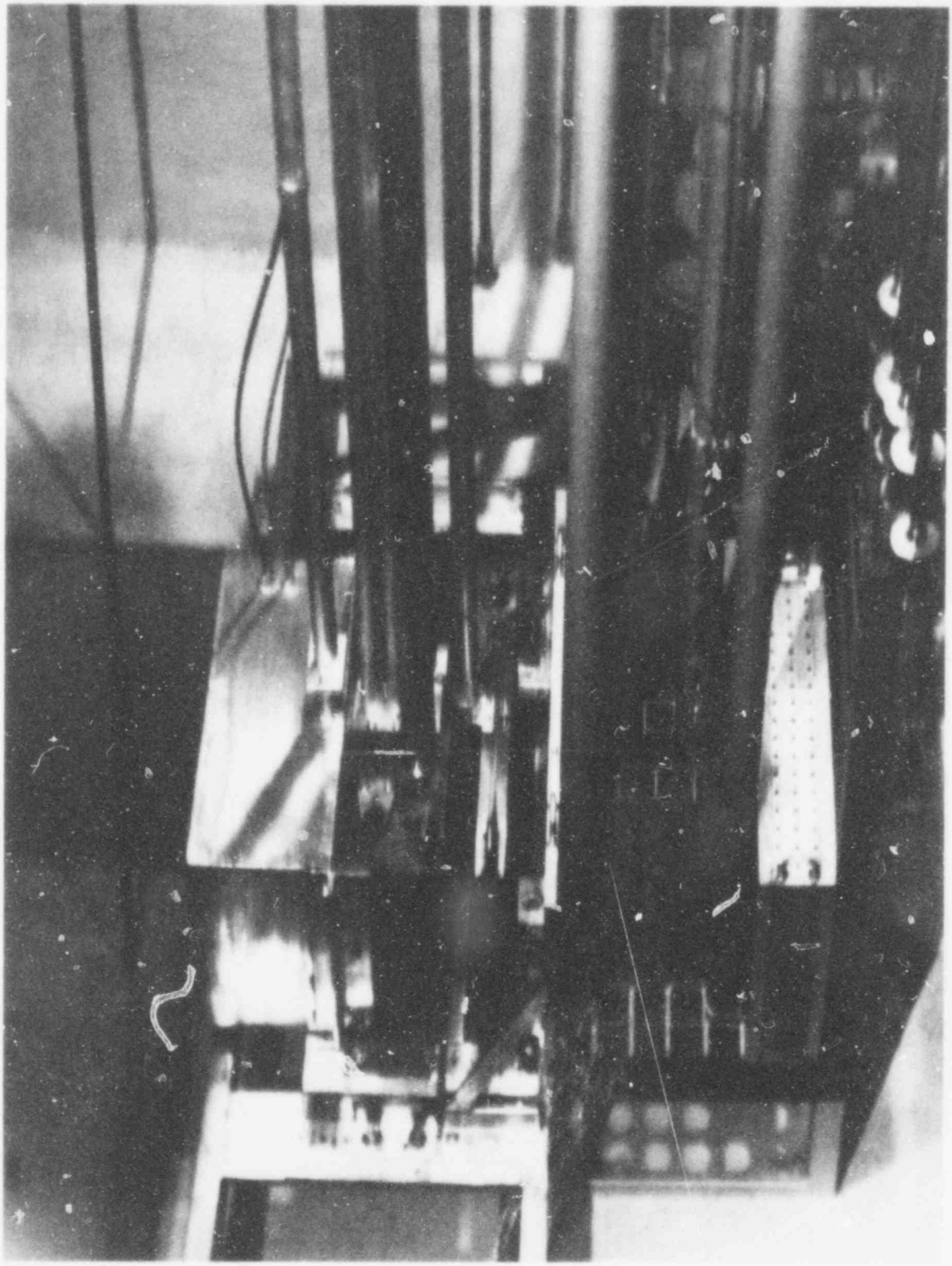

FIGURE HEDL- 6. Photograph of LWR Pressure Vessel Mockup at the PCA.
Neg. 7811291-8

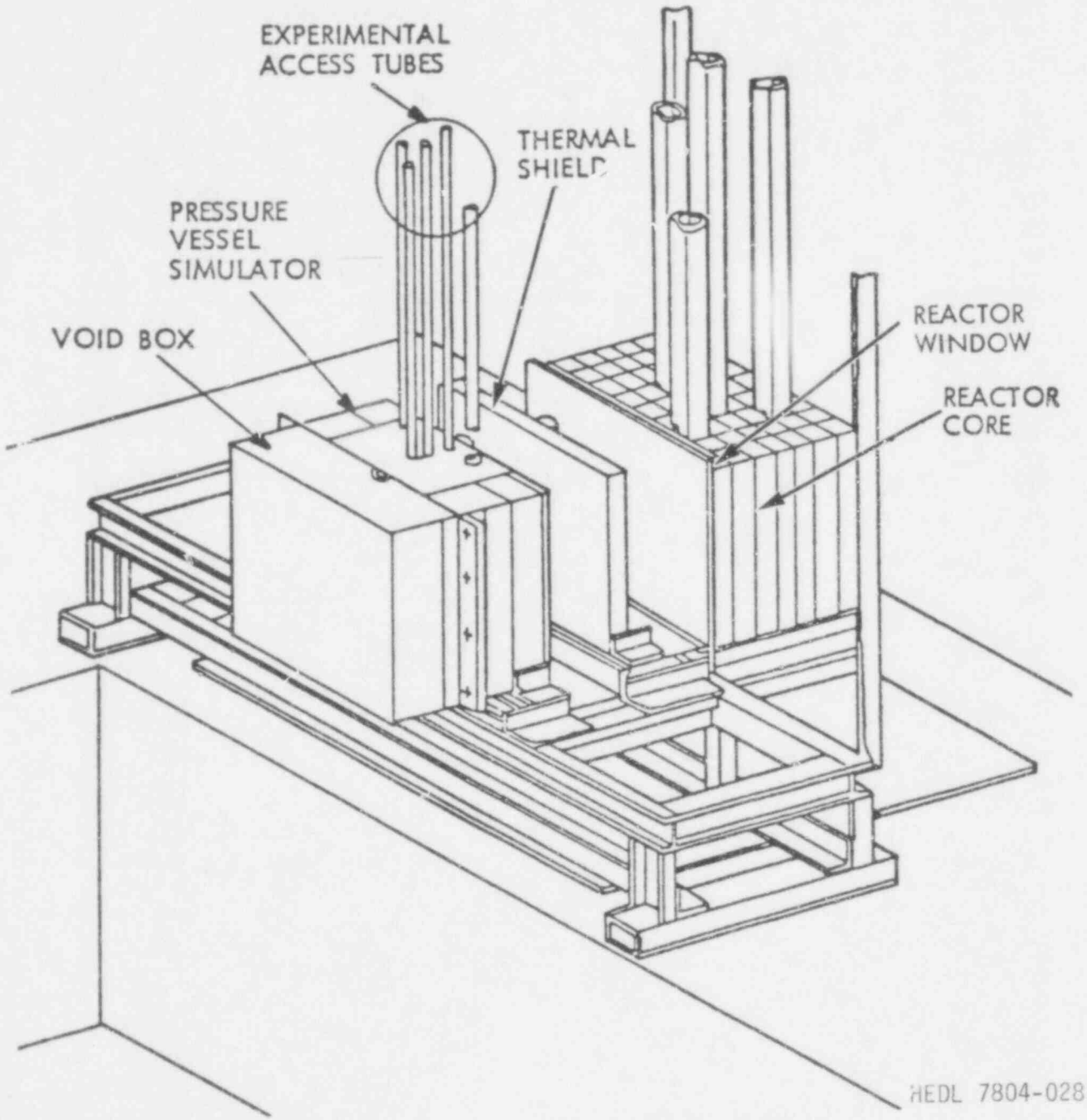

FIGURE HEDL- 7. LWR Pressure Vessel Mockup at the PCA. Neg. 7811291-1

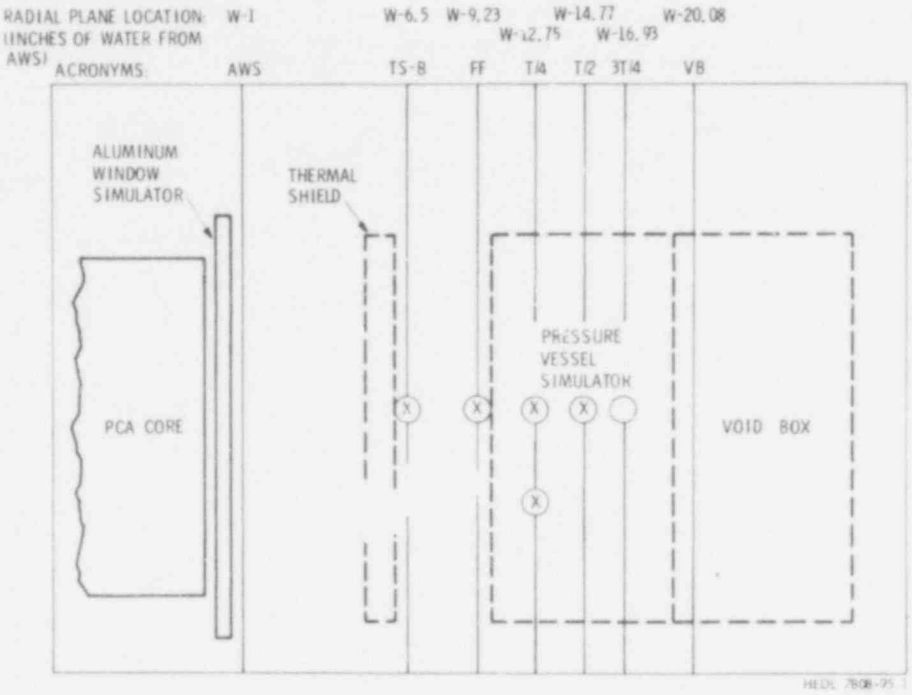

FIGURE HEDL- 8. Location of radial planes for PCA measurements in inches of water from the Aluminum Window Simulator. The dashed lines show the locations of the Thermal Shield, Pressure Vessel Simulator, and Void Box, which were not present for free-field irradiations. The acronyms are defined as follows:

PVS	Pressure Vessel Simulator
AWS	Aluminum Window Simulator
TS-B	Thermal Shield-Behind
FF	Front Face
T/4	Quarter T Location of the PVS
T/2	Half T Location of the PVS
3/4T	Three-Quarter T Location of the PVS
VB	Void Box

Neg. 7811291-2

^{137}Cs SAMPLE WITH PSD

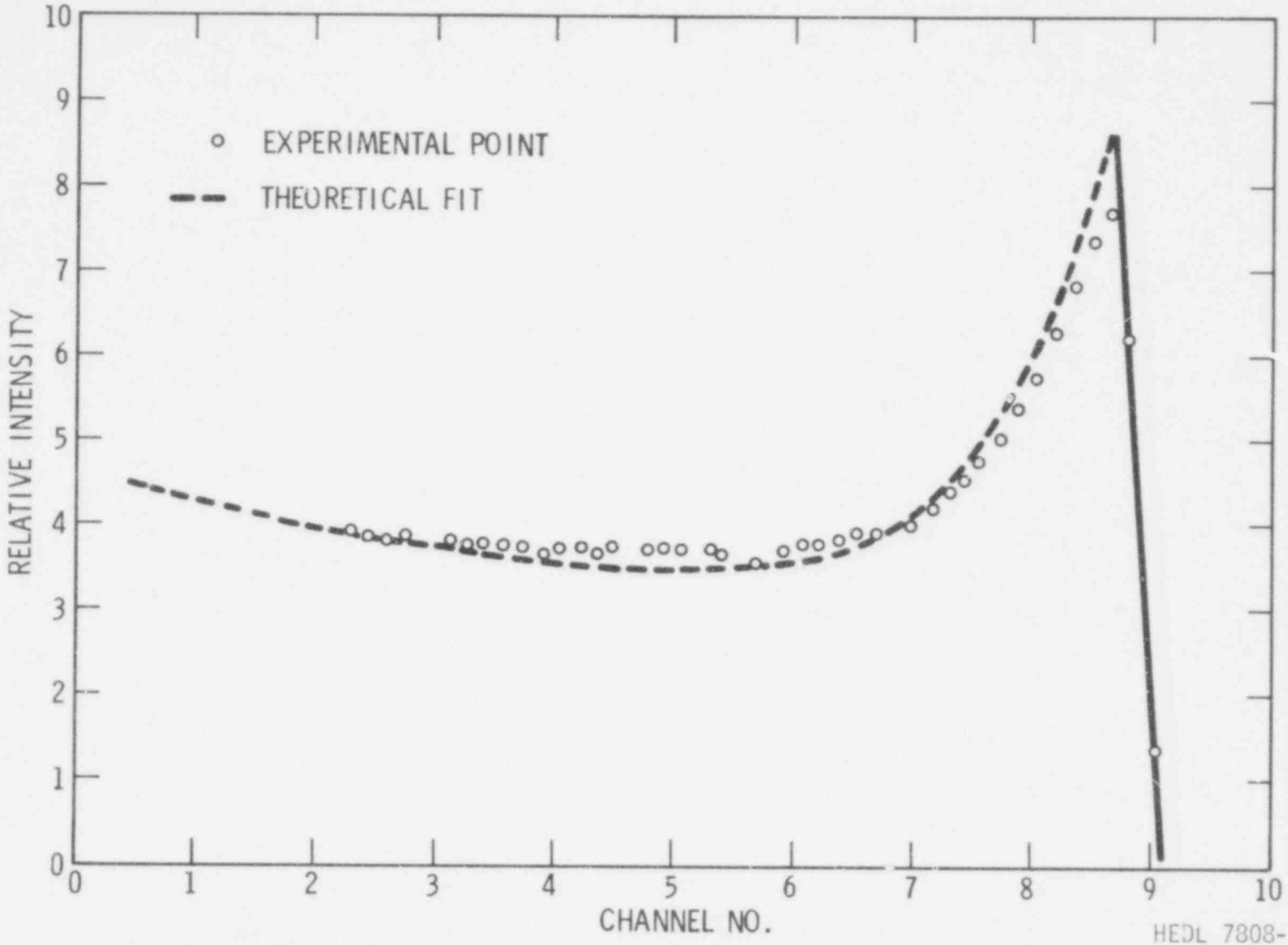

HEDL 7808-237.2

FIGURE HEDL- 9. A Comparison Between the Experimental (O) and the Theoretical Fitted (-) ^{137}Cs Compton Recoil Electron Distribution.

Neg. 7809740-5

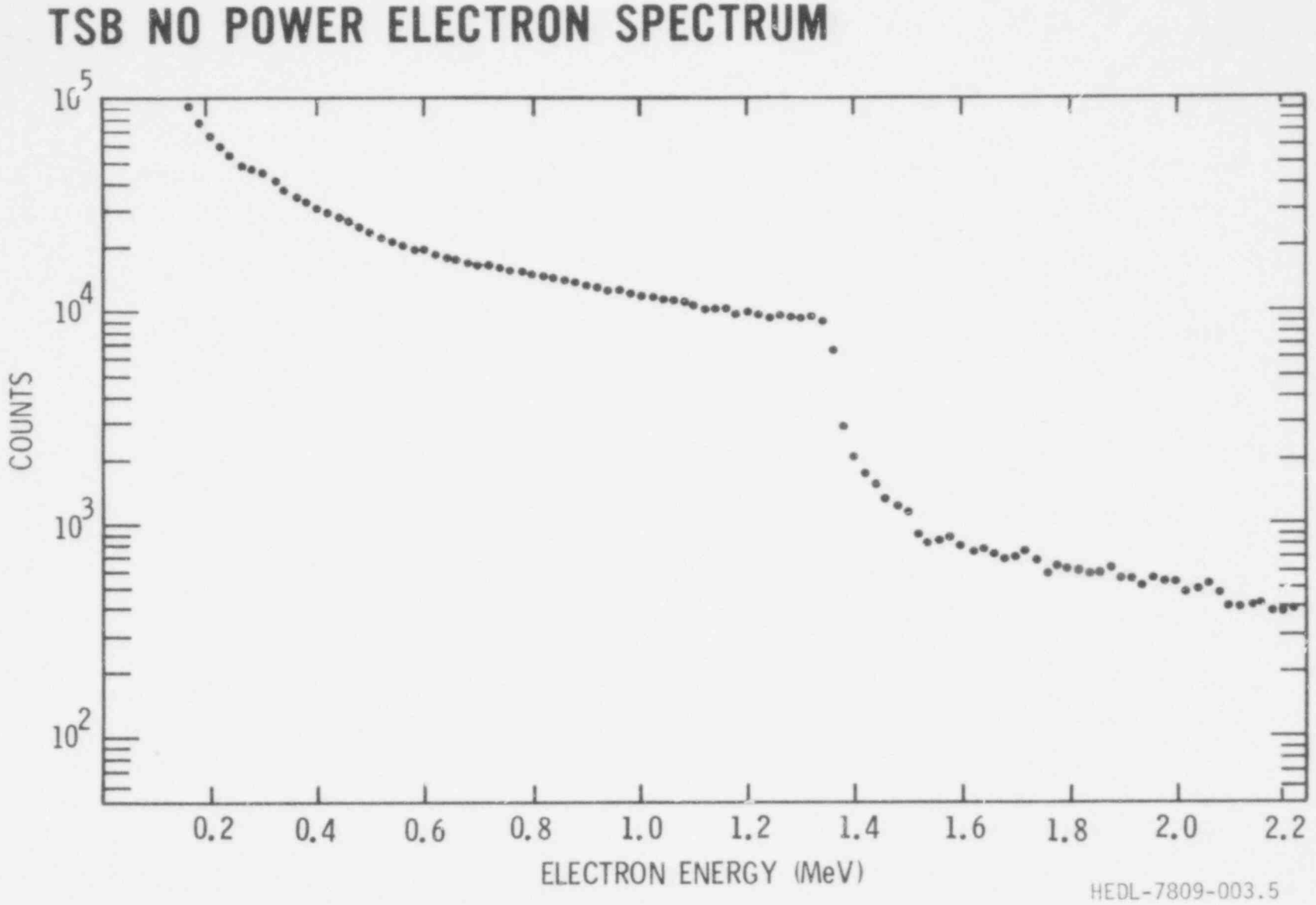

FIGURE HEDL-10. Compton Recoil Electron Spectrum at TSB Without Power.
Neg. 7811291-4

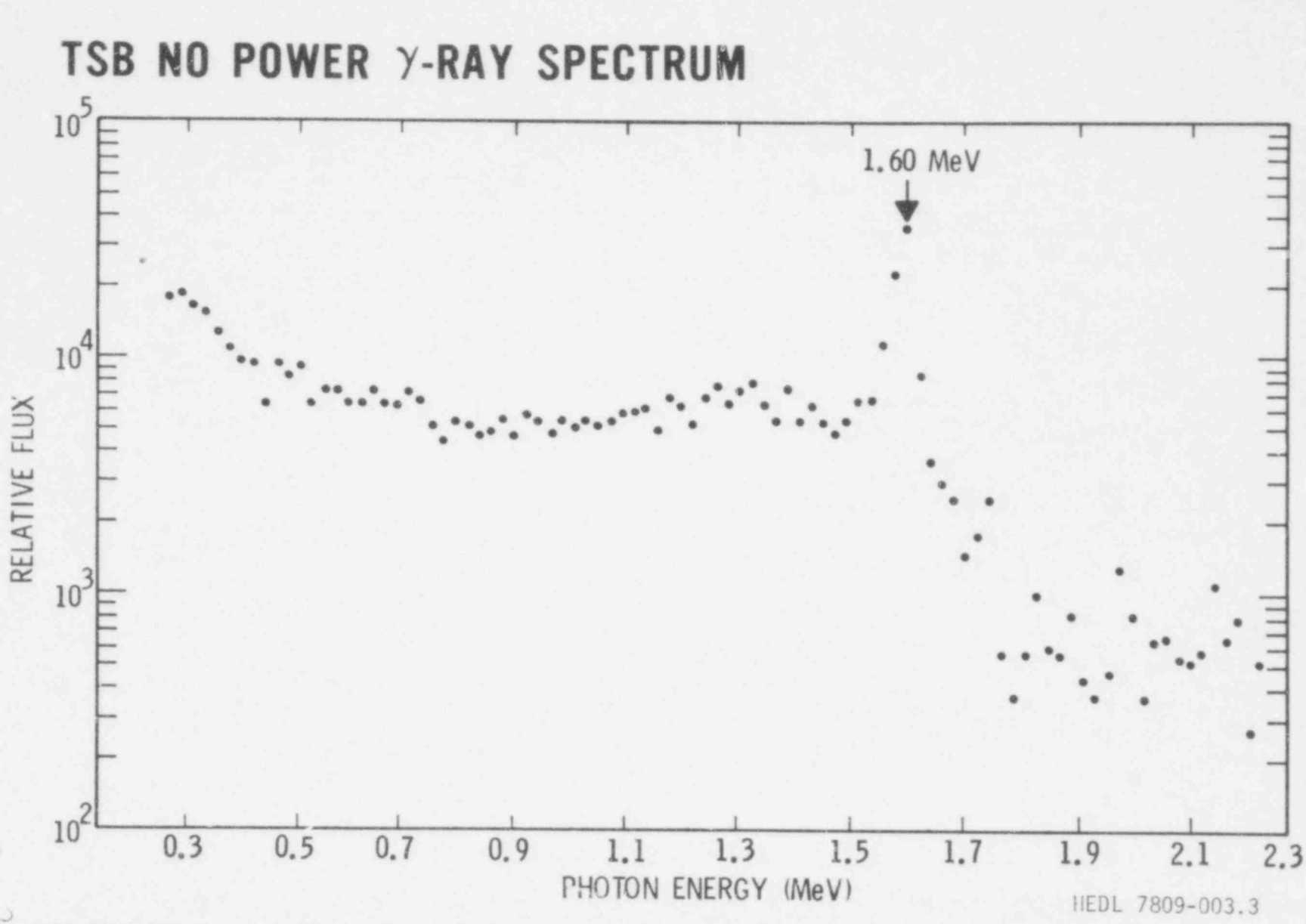

FIGURE HEDL-11. Continuous Gamma-Ray Spectrum at TSB Without Power.
Neg. 7811291-5

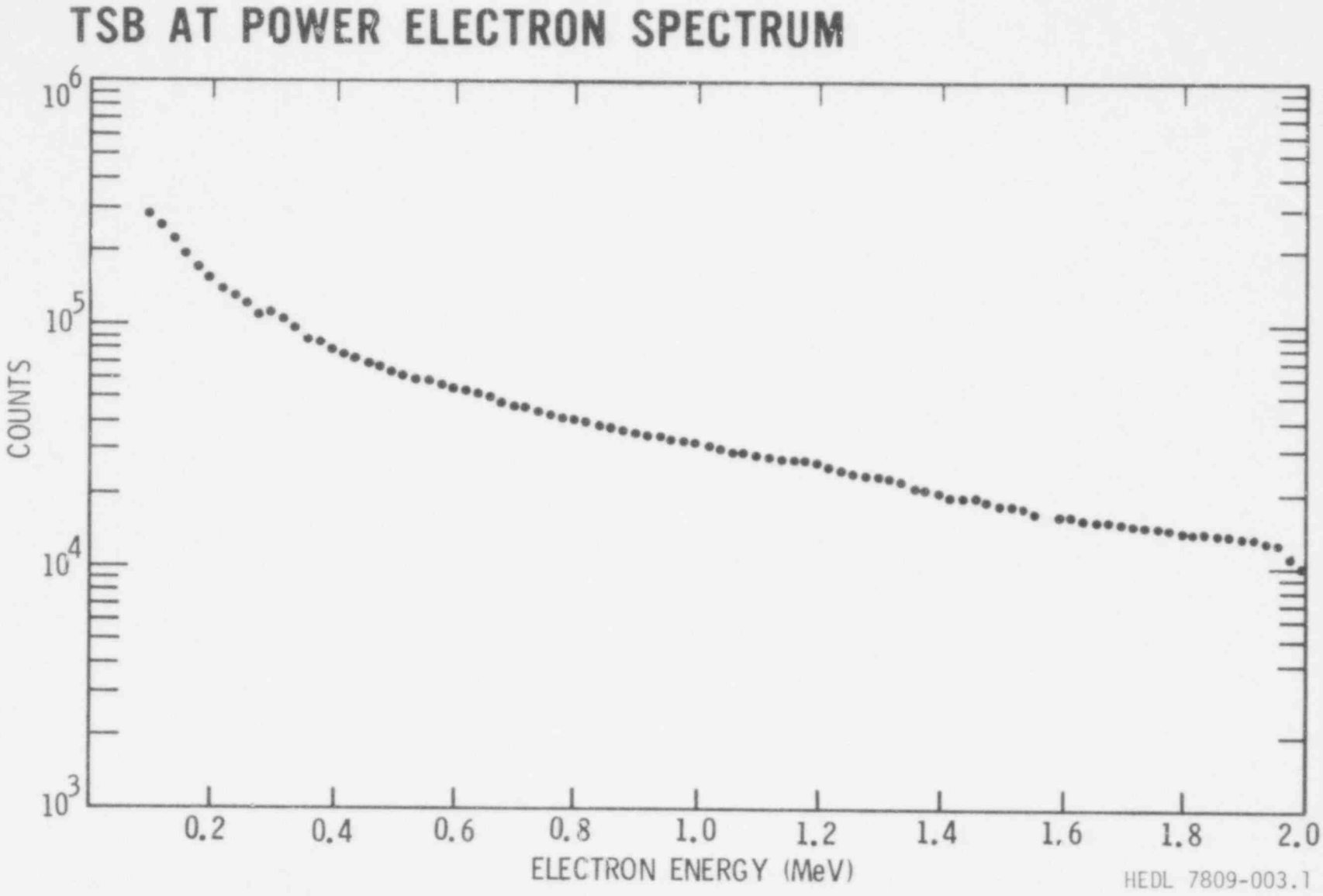

FIGURE HEDL-12. Compton Recoil Electron Spectrum at TSB With Reactor Power Level at 350 MW.
Neg. 7811291-3

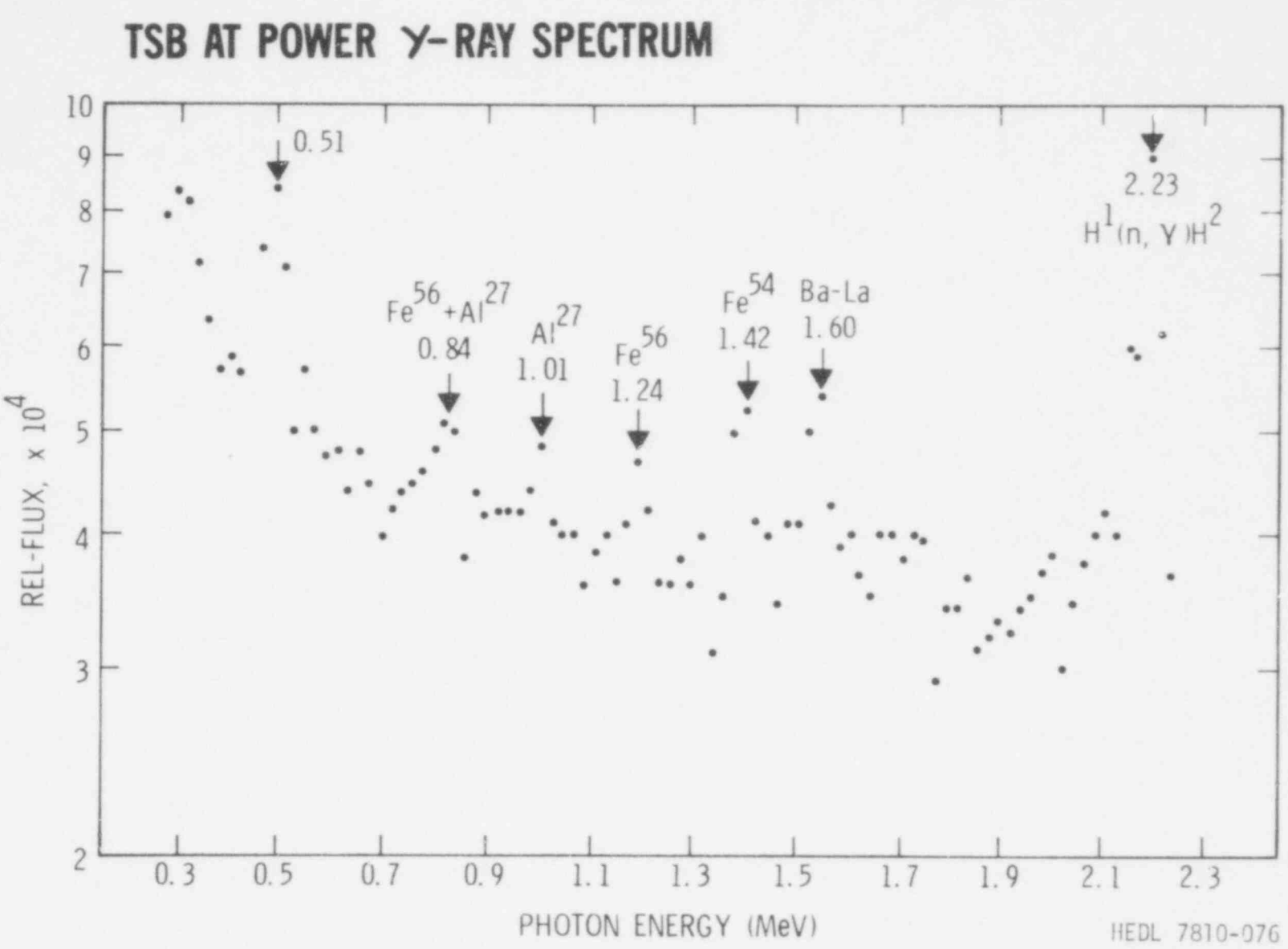

FIGURE HEDL-13. Continuous Gamma-Ray Spectrum at TSB With Reactor Power Level at 350 MW.

Neg. 7811707-1

HEDL-24

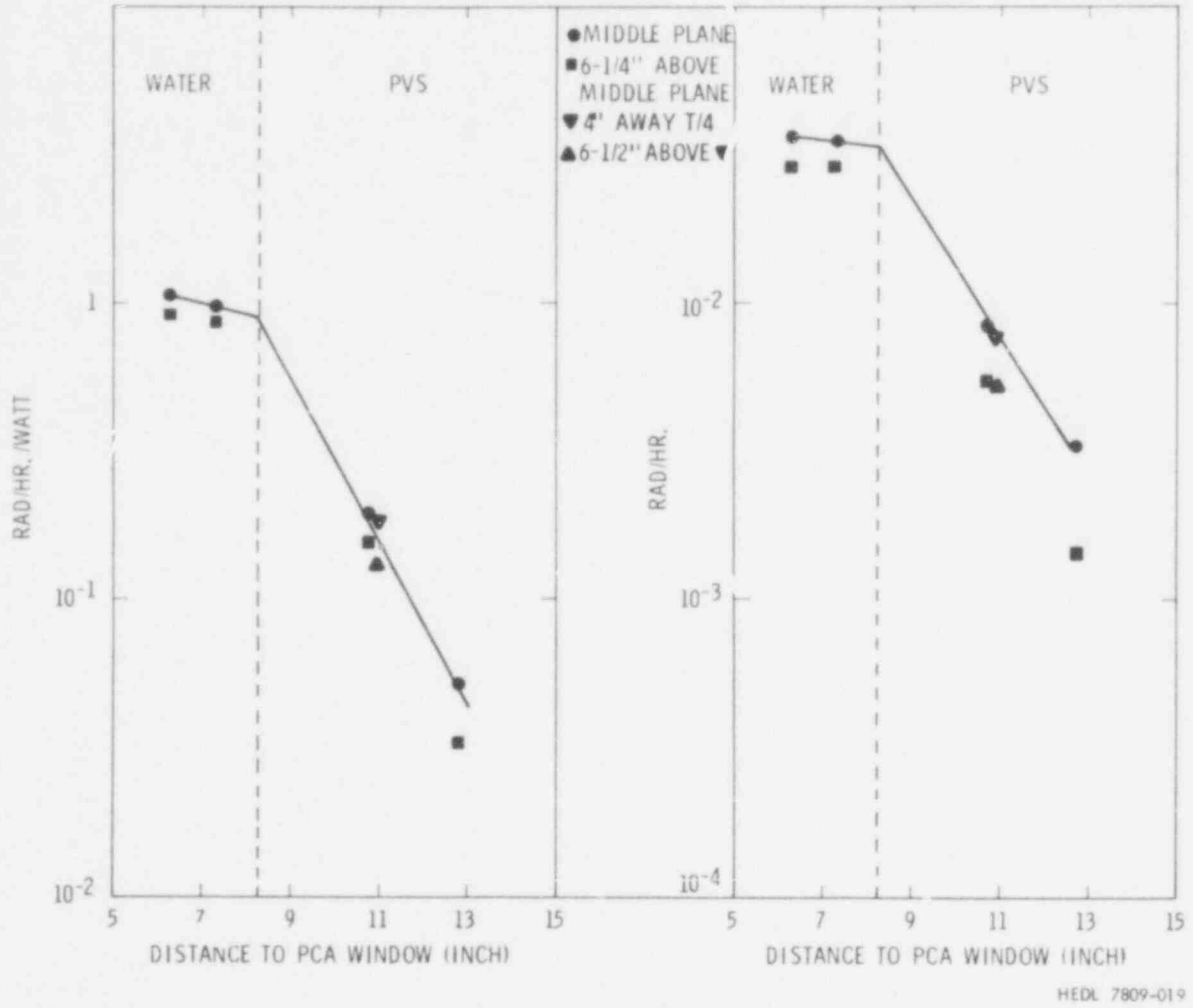

FIGURE HEDL-14. Preliminary Results of Gamma Dose Rates at PCA at Various Distances to PCA Window. Neg. 7810015-1

PREPARATION OF FISSIONABLE DEPOSITS FOR SOLID STATE TRACK RECORDER DOSIMETRY IN THE LIGHT WATER REACTOR-PRESSURE VESSEL SURVEILLANCE PROGRAM

Frank M. Ruddy
Raymond Gold
James H. Roberts*

Objective

Development of Solid State Track Recorder (SSTR) Fissionable deposit sources for dosimetry applications in Light Water Reactor-Pressure Vessel Surveillance (LWR-PVS) neutron fields.

Summary

Extensive use of SSTR in U.S. Breeder Reactor (BR), Light Water Reactor (LWR), and Magnetic Fusion Energy Reactor (MFER) programs is planned and has been described in recent reports.[1,2] In addition to the high uniformity required for such fissionable deposits,[3] extension of high accuracy SSTR techniques to high fluence requires the production of deposits that are of very low mass. Better than 1% unifomity and better than 1% absolute mass accuracy must both be accomplished. Consequently, the ability to perform accurate SSTR dosimetry at high fluence depends crucially upon the quality of these fission deposits.

Accomplishments and Status

The target thicknesses prepared for the Browns Ferry 3 (BF 3) irradiation and the planned target thickness for the McGuire I irradiation are shown in Tables HEDL-1 and -2, respectively. An electroplating procedure[4] has

*Consultant, Macalester College, Department of Physics and Astronomy, St. Paul, Minnesota 55105.

been adapted for producing deposits in the required mass range using non-quantitative deposition of the actinide isotope from an organic solvent onto a nickel backing. For ^{239}Pu, a linear dependence of source thickness versus deposition potential was found in the range from 0.08 nanograms/cm^2 to 1.58 nanograms/cm^2, as shown in Figure HEDL-15. The dependence of source thickness upon time duration of the deposition was approximately linear below 1.5 nanograms/cm^2 at 230 volts deposition potential, but extremely short times are required for the lightest deposits making variation of the deposition potential a more attractive alternative for preparation of the deposits. For ^{237}Np, a slight deviation from linearity of source thickness versus deposition potential was found above 200 nanograms/cm^2, but still a smooth dependence was found up to 1.6 μgms/cm^2 (see Figures HEDL-15 and -16).

To a first approximation Th, U, Np, and Pu behave identically in this plating procedure (due to the similarity of the properties of the M [IV] oxidation state of these actinides), and the same procedure has been used for Th and U.

The ^{237}Np, ^{239}Pu, and ^{232}Th deposits produced have been tested for uniformity by α-autoradiographic techniques using plastic SSTR. In many cases, deviations from uniformity have been found to be less than 5% and further testing is in progress.

Mass analysis has also begun for these deposits. Alpha spectrometry, mass spectrometry and spiking techniques have been and are being developed for these mass analyses. In the case of the uranium deposits, ^{237}U is being used as a γ-ray spike.

Fissionable deposits have been prepared and encapsulated for inclusion in the BF 3 cavity irradiation and absolute mass assays and uniformity measurements have been performed for these deposits (Table HEDL-1).

Expected Accomplishments

Alpha particle autoradiographs have been performed on the Browns Ferry 3 deposits, using plastic SSTRs. These autoradiographs are being analyzed for uniformity and the presence of impurity alpha emitters; these results are forthcoming. The use of alpha autoradiography as an absolute mass assay technique (with better than 1% absolute accuracy) will be investigated by comparing the results of the alpha autoradiographs with the results of conventional mass analyses.

Production of electrodeposits for the planned McGuire I irradiation will begin in order to meet the June 1979 loading deadline.

TABLE HEDL-1

SOURCE MASSES FOR THE BROWNS FERRY 3 EXPOSURE

Nuclide	Thickness* (ng/cm^2)
^{235}U	1.60
	1.66
	1.83
	2.36
^{238}U	48.9
	57.6
	65.8
	106.6
^{239}Pu	0.604
	0.733
	0.959
	2.19
^{237}Np	9.02
	9.69
	9.74
	26.1
^{232}Th	104
	220
	285
	445

*All deposits are 0.250-inch diameter on 0.437-inch diameter Ni backing. Loading will be in August 1978.

TABLE HEDL-2

PRELIMINARY LWR-PVS SSTR SOURCE ESTIMATES FOR McGUIRE I

Nuclide	Thickness* (ng/cm^2)	(#)
^{235}U	0.6	(4)
	6.0	(2)
	60	(1)
^{238}U	30	(4)
	300	(2)
	3×10^3	(1)
^{239}Pu	0.6	(4)
	6.0	(2)
	60	(1)
^{237}Np	6	(4)
	60	(2)
	600	(1)
^{232}Th	120	(4)
	1.2×10^3	(2)
	12×10^3	(1)

*All deposits 0.250-inch diameter on 0.438-inch diameter, 5 mil Ni backing. Required date to begin testing 3/79. Required date for PVS loading 6/79.

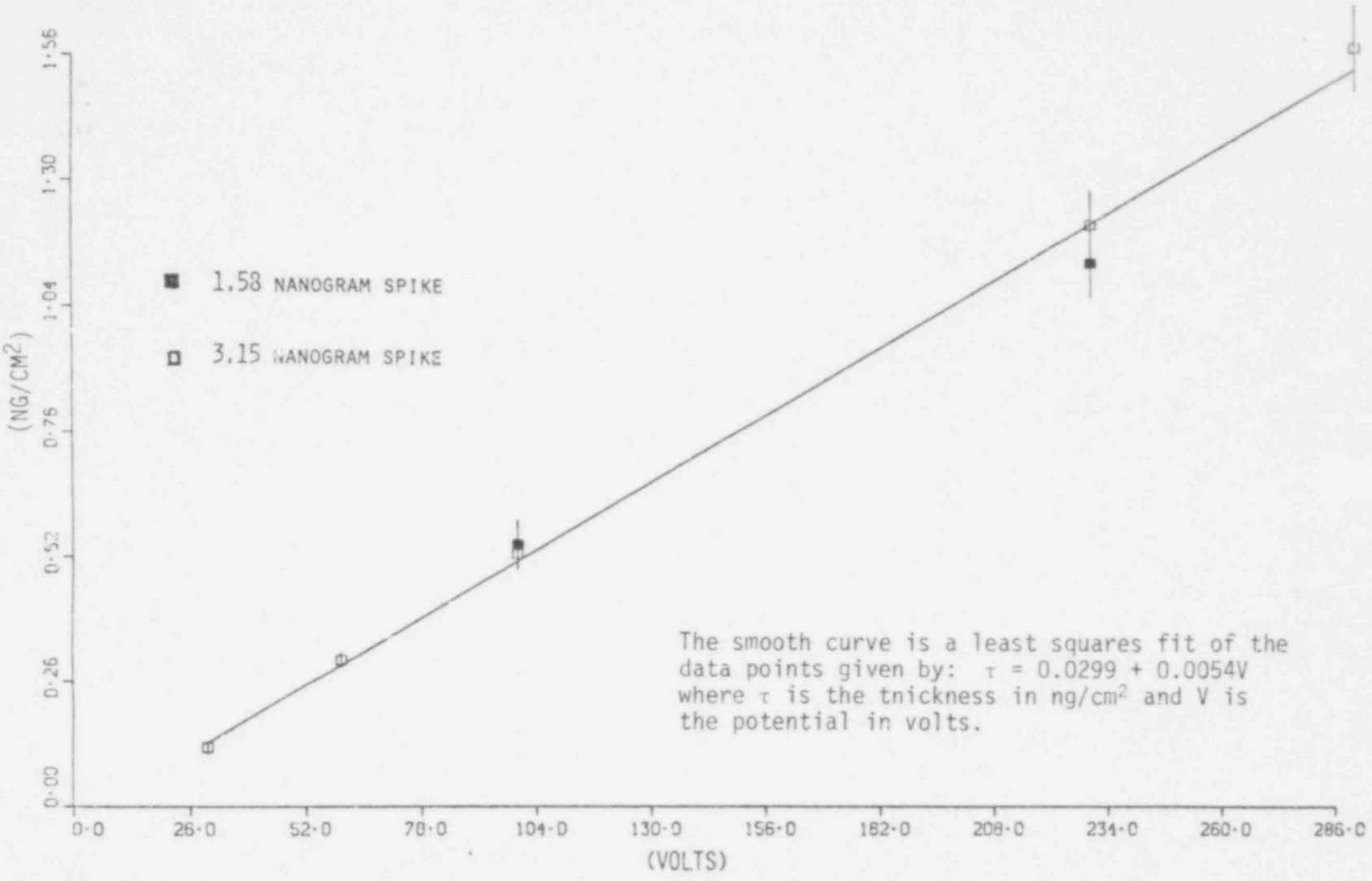

FIGURE HEDL-15. Deposit Thickness vs. Deposition Potential for ^{239}Pu.

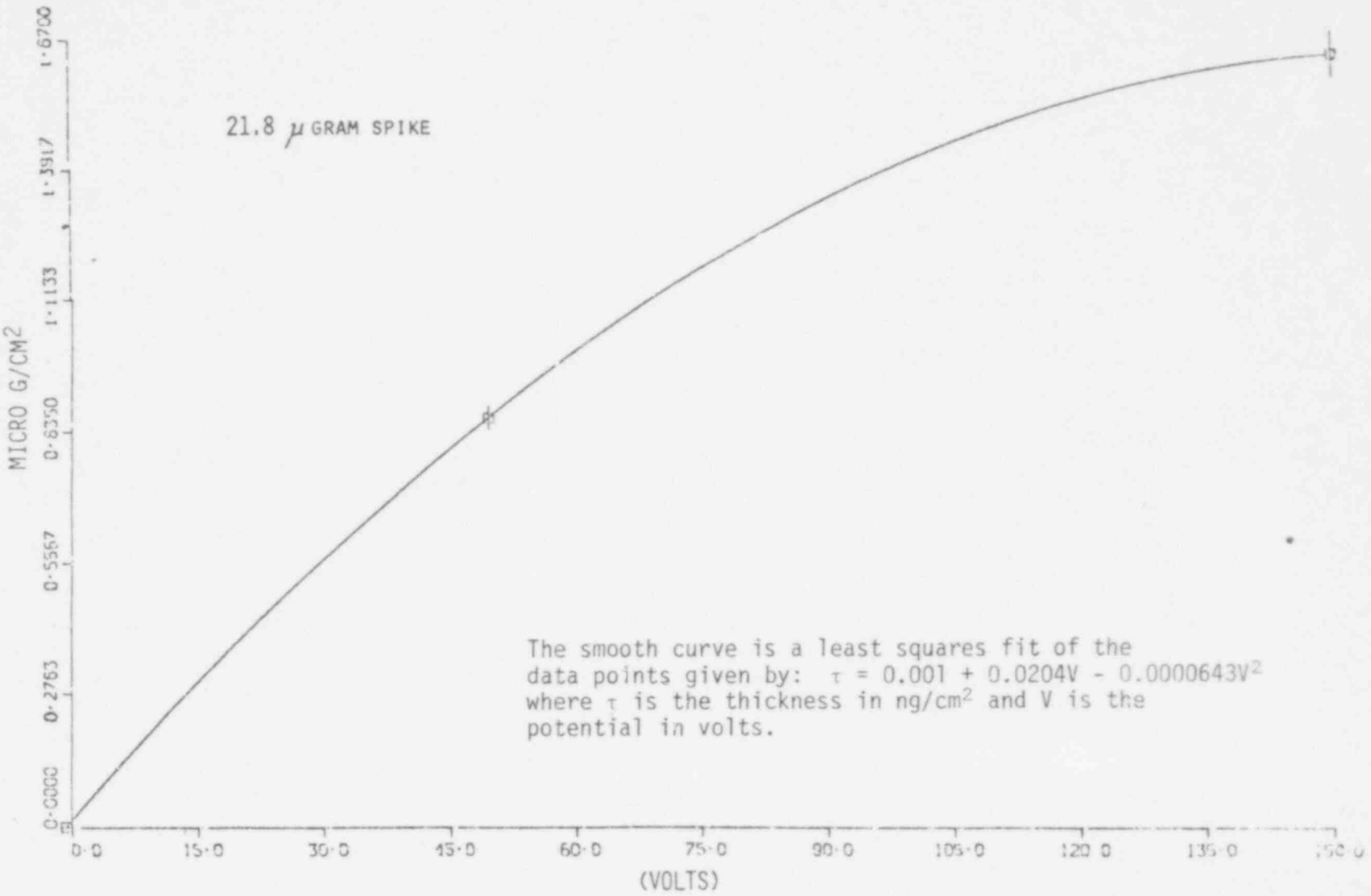

FIGURE HEDL-16. Deposit Thickness vs. Deposition Potential for ^{237}Np. A 21.8 μgram ^{237}Np spike was used.

HEDL-33

515 221

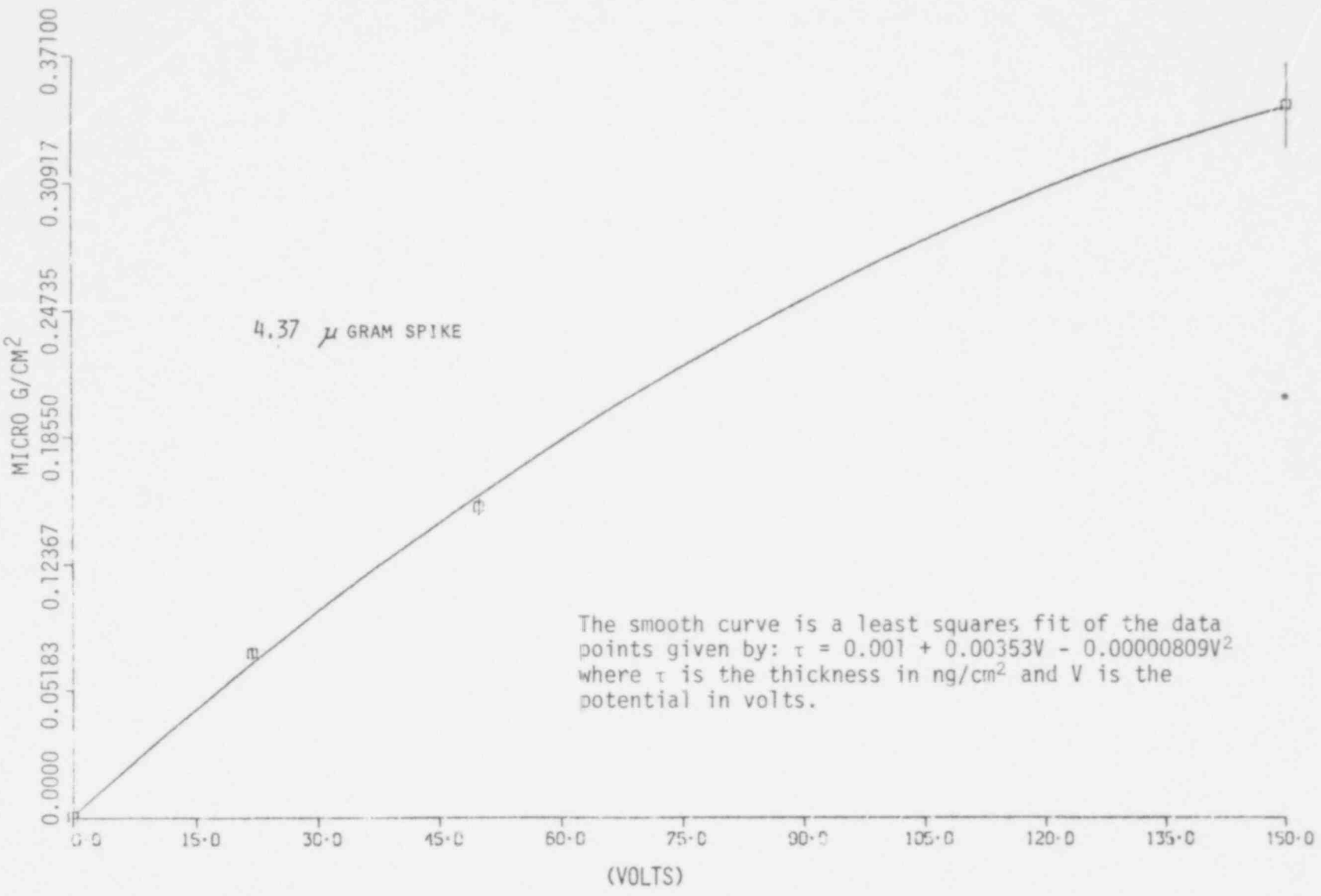

FIGURE HEDL-17. Deposit Thickness vs. Deposition Potential for ^{237}Np. A 4.37 μgram ^{237}Np spike was used.

REFERENCES

1. J. H. Roberts and R. Gold, "SSTR and Emulsion Techniques and Their Applications for FBR, LWR, and MFER Programs," Second ASTM-EURATOM Symposium on Reactor Dosimetry, Palo Alto, California (1977).

2. R. Gold, F. H. Ruddy, and J. H. Roberts, "Solid State Tracker Recorder Materials for Use in Light Water Reactor-Pressure Vessel Surveillance Exposures," 9th ASTM International Symposium on Effects of Radiation on Structural Materials, July 11-14, 1978, Richland, Washington.

3. R. Gold, R. J. Armani, and J. H. Roberts, "Absolute Fission Rate Measurements with Solid State Track Recorders," Nucl. Sci. Engr. 34, 13 (1968).

4. T. H. Handley and J. H. Cooper, "Quantitative Electrodeposition of Actinides from Dimethylsulfoxide," Analytical Chemistry 41, 381 (1969).

C. THE EFFECT OF MINOR ELEMENTS ON THE IRRADIATION EMBRITTLEMENT OF WELD METAL-II

G. L. Guthrie

Objective

The objective of this work is to provide statistical information about the effect of minor elements on the shift of the nil ductility temperature of Light Water Reactor-Pressure Vessel (LWR-PV) weld metal under irradiation. The information thus obtained is useful in the preparation of some ASTM Standard Practices required under the LWR Surveillance Dosimetry Program. The immediate objective of this report is to list the embrittlement sensitivity coefficients in terms of weight percent, rather than atomic percent as was done in a previous quarterly report, and to examine the statistical significance of some coefficients in greater detail.

Summary

In a previous report[1], a simple linear expression was used to provide a relationship between weld metal chemistry and the irradiation induced shift in the nil ductility temperature of irradiated weld metal. The linear expression contains a number of adjustable coefficients which show how concentrations of individual minor alloying elements contribute to the total temperature shift. These adjustable coefficients were evaluated by a "least squares" technique using data from irradiations of 36 different weld metal alloys. Confidence limits for the coefficient values were presented. The current report gives embrittlement sensitivity coefficients in terms of weight percent, rather than atomic percent, and enlarges on the analysis of the statistical significance of the parameters. Use of additional statistical tests show that the parameters for Cu, Mn, P, Mo, Ni, Cr, and V all show evidence of being statistically significant.

Accomplishments and Status

In a previous quarterly report[1], data assembled by Biemiller et al[2] were analyzed to show that several alloying elements affect the irradiation embrittlement sensitivity[3] of pressure vessel steels. The data[2], from 36 weld metal alloys irradiated at 288°C were presented in a normalized form to show shift in nil ductility temperature (evaluated from Charpy tests) after irradiation to 3×10^{19} n/cm^2 (E>1.0 MeV). Data from irradiation to fluences other than 3×10^{9} n/cm^2 (E>1.0 MeV) were adjusted by the authors[2], using an assumed relation where nil ductility temperature shift was proportional to the .43 power of the fluence attained in the irradiation. In the earlier quarterly report[1], data were analyzed using an assumed relation of the form

$$\begin{aligned}\Delta(\text{NDTT}) = {} & A_C \cdot (\text{At \% C}) + A_{Mn} (\text{At \% Mn}) \\ & + A_P \cdot (\text{At \% P}) + A_S \cdot (\text{At \% S}) + A_{Si} \cdot (\text{At \% Si}) \\ & + A_{Ni} \cdot (\text{At \% Ni}) + A_{Cr} \cdot (\text{At \% Cr}) + A_{Mo} \cdot (\text{At \% Mo}) \\ & + A_{Cu} \cdot (\text{At \% Cu}) + A_V \cdot (\text{At \% V}) + \text{Constant.}\end{aligned} \qquad (1)$$

In the expression above, the coefficients A_C, A_{Mn}, etc., are adjustable parameters for carbon, manganese, and other minor alloying elements, evaluated by a linear least-squares technique so as to obtain a best fit to the data. Normalized data consist of tabulations of the chemical composition of the welds and the associated shift in nil ductility temperature caused by irradiation to 3×10^{19} n/cm^2 (E>1.0 MeV).

In the previous report, the chemical compositions were entered into calculations as atomic percent alloy additions.

Since the chemical analysis is commonly given in weight per cent, and Regulatory Guide 1.99 discusses[4] a problem similar to the present one using weight per cent for chemical analysis, Eq(1) has been modified to the form of Eq(2) which used weight per cent for the alloy concentration terms.

$$(NDTT) = A_C \cdot (Wt\ \%\ C) + A_{Mn} \cdot (Wt\ \%\ Mn) + A_P \cdot (Wt\ \%\ P) + A_S \cdot (Wt\ \%\ S)$$
$$+ A_{Si} \cdot (Wt\ \%\ Si) + A_{Ni} \cdot (Wt\ \%\ Ni) + A_{Cr}\ (Wt\ \%\ Cr) + A_{Mo} \cdot (Wt\ \%\ Mo) \qquad (2)$$
$$+ A_{Cu}\ (Wt\ \%\ Cu) + A_V \cdot (Wt\ \%\ V) + Constant$$

This will allow better comparison of results to Reg Guide 1.99 and facilitate utilization of the results of the analysis.

A standard least squares technique[5] has been used to analyze the 26 data points of Pickering and Byrne using all the terms of Eq(2) and the results are shown in Table HEDL-3. In addition to the analysis with the full set of elements, Eq(2) has been analyzed in an abbreviated form in several cases where various elements were eliminated from Eq(2) and the least-squares solution was found for the remaining coefficients in the abbreviated expression in each case. Table HEDL-4 shows the coefficients which resulted from this type of analysis for various combinations of assumed relevant elements. Table HEDL-5 shows the corresponding standard deviations for the coefficients found by the least-squares procedure.

The method used to choose elements (and associated parameters) for retention is the following. The full sets of elements for which chemical analysis was available was used for Case I. This case is shown in Table HEDL-3. It was assumed that elements which did not actually affect the embrittlement process would have poorly determined coefficients, since there would be a poor correlation between the concentrations of such elements and the nil ductility temperature shift. Therefore, it seemed reasonable to rank the elements based on the fractional uncertainty in the least-squares embrittlement coefficient found for the full set of elemental concentrations, (Case I). Subsets of elements could be selected, starting with a few of the elements with the most accurately determined coefficients, and enlarging the set by adding elements

in order, using the previous ranking (Column 5 of Table 3, Case I) as a guide to a reasonable sequence of additional elements and associated parameters.

The decision on how large a set to use as an ultimate optimum set can be based on a desire to obtain the minimum value for the standard deviation of the fit to the data. This might cause retention of a excessive number of parameters in a situation where the deviation of the fit had a very small decrease associated with the addition of an extra parameter, with the improvement being happenstance. The judgment of the situation just referred to can be put on the quantitative basis by the use of the "F" statistic, which will be discussed later.

TABLE HEDL-3

RADIATION EMBRITTLEMENT COEFFICIENTS FOR VARIOUS ELEMENTS
IN AN EXPRESSION CONTAINING TEN ELEMENTS PLUS A CONSTANT TERM

Element (or Constant term)	Coefficient in $^{o}C/Wt\%$ at 3×10^{19} n/cm^2 (E>1.0 meV)	Standard Deviation $^{o}C/Wt\%$	Fractional Uncertainty (Col 3/Col 2)	Reliability Rank (Based on Col 4)
C	.1246E+03	.2303E+03	1.85	9
Mn	-.5977E+02	.2718E+02	.45	4
P	.4066E+04	.1688E+04	.41	3
S	-.1610E+03	.3225E+04	20.	11
Si	-.1907E+02	.5644E+02	2.63	10
Ni	.2267E+02	.1275E+02	.56	6
Cr	.3517E+02	.2134E+02	.61	7
Mo	-.2244E+03	.8264E+02	.38	2
Cu	.3485E+03	.5758E+02	.17	1
V	.3411E+03	.4872E+03	1.4	8
Constant	.1613E+03 (^{o}C)	.8987E+02 (^{o}C)	.56	5

TABLE HEDL-4

RADIATION EMBRITTLEMENT COEFFICIENTS FOR SEVERAL COMBINATIONS OF ELEMENTS (^{o}C/Wt % at 3×10^{19} n/cm^2 (E>1.0 MeV))

Element	Case I	Case II	Case III	Case IV	Case V	Case VI	Case VII	Case VIII	Case IX
C	.1246E+03								1478E+03
Mn	-.5977E+02				-.7843E+02	-.5716E+02	-.6148E+02	-.6310E+02	-.5783E+02
P	.4066E+04	.3248E+03		.2517E+04	.3535E+04	.3763E+04	.3553E+04	.3316E+04	.3793E+04
S	-.1610E+03								
Si	-.1907E+02								
Ni	.2267E+02					.2310E+02	.1848E+02	.1813E+02	.2287E+02
Cr	.3517E+02						.2832E+02	.2753E+02	.3507E+02
Mo	-.2244E+03		-.6415E+02	-.4514E+02	-.1018E+03	-.9201E+02	-.2019E+03	-.2234E+03	-.2259E+03
Cu	.3485E+03	.4417E+03	.4186E+03	.4079E+03	.3861E+03	.3478E+03	.3540E+03	.3544E+03	.3491E+03
V	.3411E+03							.4825E+03	.3812E+03
CONSTANT	.1613E+03	.7019E+00	.7937E+02	.4304E+02	.1661E+03	.1167E+03	.1745E+03	.1840E+03	.1513E+03
Sum of Squares of Residuals	.2929E+05	.5624E+05	.5754E+05	.5334E+05	.4072E+05	.3469E+05	.3171E+05	.3027E+05	.2971E+05
*Standard Deviation	.3423E+02	.4128E+02	.4176E+02	.4083E+02	.3624E+02	.3401E+02	.3307E+02	.3288E+02	.3317E+02
**Degrees of Freedom	25.	33.	33.	32.	31.	30.	29.	28.	27.

* Standard deviation data, given by ((sum of squares of residuals)/(degrees of freedom))$^{0.5}$.

**Degrees of freedom defined as number of data points minus number of adjustable parameters.

TABLE HEDL-5

STANDARD DEVIATIONS OF ELEMENT COEFFICIENTS FOR SEVERAL COMBINATIONS OF ELEMENTS

Element	Case I	Case II	Case III	Case IV	Case V	Case VI	Case VII	Case VIII	Case IX
C	.2303E+03								.2069E+03
Mn	.2718E+02				.2530E+02	.2550E+02	.2494E+02	.2483E+02	.2612E+02
P	.1688E+04	.1502E+04		.1586E+04	.1445E+04	.1360E+04	.1329E+04	.1337E+04	.1505E+04
S	.3225E+04								
Si	.5644E+02								
Ni	.1275E+02					.1012E+02	.1023E+02	.1018E+02	.1222E+02
Cr	.2134E+02						.1716E+02	.1708E+02	.2020E+02
Mo	.8264E+02		.3280E+02	.3423E+02	.3545E+02	.3354E+02	.7417E+02	.7605E+02	.7681E+02
Cu	.5758E+02	.5969E+02	.6546E+02	.6436E+02	.5756E+02	.1788E+03	.5513E+02	.5481E+02	.5579E+02
V	.4872E+03							.4176E+03	.4445E+03
CONSTANT	.8987E+02	.1704E+02	.2876E+02	.3626E+02	.5110E+02	.5259E+02	.6197E+02	.6216E+02	.7758E+02

Units are $(^{0}C/Wt\ \%)^{2}$

5/5 229

The ranking of the coefficients from Case I was found to be Cu, Mo, P, Mn, additive constant, Ni, Cr, V, C, Si, and S, as shown in Table HEDL-3. In the computations the additive constant was included in all cases. This is not in complete harmony with the theory just discussed, as the constant should be included in the proper sequence on the same basis as the rest of the parameters, but the discrepancy turned out not to be important, since the minimum value for the standard deviation of the data was observed for a set of parameters which was larger than the smallest set which included the additive constant taken in proper sequence.

Most of the various subset "cases" shown in Tables HEDL-4 and HEDL-5 are based on the previously mentioned ranking. Cases III, IV, V, VI, VII, VIII and IX show the effects of adding the elements in sequence, in order of rank. Case I is out of sequence in the table, since it is the full set, and Case II is not a proper member of the sequence but was included because of its similarity to Reg. Guide 1.99.

Tables HEDL-4 and -5 show that statistically derived "best values" for coefficients depend upon the choice of the "relevant" elements. This is quite obvious from comparison of the molybdenum coefficient as found in Case IV with that found in Case VIII. This phenomenon occurs because the alloys were not specifically designed to produce data which would generate partial derivatives. Such design would require varying the composition of each element (vs. iron) individually, with the other compositions held constant. In the available alloys, certain pairs of elements vary in composition in coordinated patterns which may be accidental or the result of metallurgical facts. In the assumed linear relation between composition and temperature shift, deletion of one member of a pair whose occurrence is correlated would change the value of the coefficient of the remaining pair member. In the statistical analysis, this phenomenon appears as a significant absolute value for the covariance term in the more complete case with both elements present. Since the values of the parameters depend on the choice of variables, decisions must be made as to what constitutes a reasonable set of independent variables. Keeping all available parameters in the equation is

not necessarily the best choice, as this would increase the computation in implementation of the procedure of predicting temperature shifts. It also reduces the excess of the number of data points over the number of parameters (called degrees of freedom). For elements that do not control the temperature shift, the inclusion of unneeded parameters slightly reduces the reliability of the final formula.

Examination of the last two rows of Table HEDL-4 shows that going from Case I to Case VIII has not materially increased the sums of squares of residuals, while actually decreasing the square root of the sum of squares of residuals per degree of freedom. This last item measures scatter on a basis of root mean-square deviation per excess data point and is the standard deviation of the fit to the data. "Excess data point" means the excess above the minimum number needed to determine a set of values for the coefficients. Judging by the values in the last two rows of Table HEDL-4, Cu and P do not constitute an ideal set of independent chemical variables for analyzing the Biemiller data. On the other hand, the set in Case VIII seems excellent. The comparatively low value of 30,270 for the total of the sum of squares of residuals indicates a good fit to data, while the comparatively low value in the last row indicates that the fit has been achieved by use of meaningful variables. In going from Case VIII to Case IX, the addition of C to the set of elements reduces the sum of the squares of the residuals but increases the standard deviation. Therefore, it is obvious that the optimum set of parameters is no larger than the one shown in Case VIII, for the given input data.

When sampling from a normally distributed population, it is possible to calculate a number

$$Z_n^2 = \sum_{i=1}^{n} \left(\frac{y_i - \mu}{\sigma} \right)^2$$

by randomly choosing n population members at random. If μ is unknown, a similar Z^2 can be calculated using n + 1 members and applying the formula

$$Z_n^2 = \sum_{i=1}^{n+1} \left(\frac{y_i - \bar{y}}{\sigma} \right)^2$$

where $\bar{y}$ is the average value of dependent variable for the n + 1 members chosen. The value of Z^2 will change from one statistical sampling experiment to another and will have a probability distribution varying smoothly from zero to infinity and peaked near $Z^2 = n$. This is called a Chi-squared distribution of degree n. Independently constructing Z^2 values with n and m members from two populations, and taking the ratio $(Z_n^2/n)/(Z_m^2/m)$ produces a number "F" which is randomly distributed and peaked near unity. The shape of the distribution depends on n and m, and the distribution is called an "F" distribution of n and m, written as F(n,m). It is possible to test for the significance of added parameters in a linear expression using formulas involving the F statistic. Basically, the idea behind the formula is the following: When an additional parameter is added, the degrees of freedom factor is decreased by unity, so the situation is similar to losing a data point, or reducing n by unity in constructing a Chi-square number. If the added parameter is really significant, the value of Chi-square per degrees of freedom should show a noticeable shift. What constitutes a noticeable shift depends on the magnitude of Chi-square per degree of freedom. That is, the ratio of the shift to the value should be large enough to be improbable. An F test based on logic somewhat similar to that given above is suggested by Mendenhall and Schaefer.[6] These authors state that for two different parameter levels, the statistic

$$G = \frac{(SSE1 - SSE2)}{SSE2} \times \frac{DF}{Delta\ P}$$

has a distribution of the F (ΔP,DF) type. In the formula above, SSE1 is the sum of the squares of the errors for the data-fitting with the smaller number of parameters, and SSE2 is the similar term for the more complex fitting

routine. Delta P is the increase in number of parameters, and DF is the number of degrees of freedom (excess of data points over parameters) in the complex case. If the additional parameters are significant, the number G should be improbably large and should fall in the upper tail of the F distribution. This recipe has been used to test the significance of added parameters in several cases. The results are shown in Table HEDL-6.

TABLE HEDL-6

F TEST - SIGNIFICANCE OF ADDED PARAMETERS

Elements (or additive constant) Assumed Relevant in Fit With Reduced Number of Parameters	Parameters Added for Additional Elements	Confidence Level that Change is Significant
Constant Cu, Mo.	P	87.7%
Constant Cu, Mo, P	Mn	99.59%
Constant Cu, Mo, P, Mn	Ni	97.04%
Constant Cu, Mo, P, Mn, Ni	Cr	89.04%
Constant Cu, Mo, P, Mn, Ni, Cr	V	74.18%

It appears from Table HEDL-6 that there is justification for choosing the set of elements used in Case VIII (the most complete set shown in Table HEDL-6) over the sets having smaller numbers of parameters.

A computer program has been written to diagonalize the covariance matrix for the embrittlement problem. That is, the program finds psuedo-elements whose concentrations are linear combinations of the actual elements, such that the pseudo-elements have independent embrittlement coefficients.

The linear combinations, the embrittlement coefficients, and the variance of the coefficients are shown in Tables HEDL-7 and -8.

TABLE HEDL-7

LINEAR COMBINATIONS OF CONCENTRATIONS OF ELEMENTS RESULTING IN A DIAGONALIZED COVARIANCE MATRIX

Linear Combination Designation	Combination C	Mn	P	S	Si	Ni	Cr	Mo	Cu	V	CN
LC1	-.06	.00	-.99	.08	-.00	-.00	-.00	-.01	.01	.11	.02
LC2	.12	.01	-.13	-.16	.02	.00	.00	.04	.00	-.97	-.04
LC3	.27	.02	.04	.95	.03	.01	.02	-.02	-.01	-.12	-.08
LC4	.92	.04	-.06	-.26	.10	.03	.03	-.02	-.00	.17	-.21
LC5	-.14	.12	-.01	.01	.17	.03	-.16	.74	.13	.04	-.58
LC6	-.00	.06	-.01	-.01	-.03	.07	-.08	.14	-.98	.00	-.00
LC7	.08	.13	-.00	.00	-.97	.04	.06	.17	.06	.00	-.06
LC8	-.19	.54	.00	-.02	.01	.09	.23	-.52	-.05	-.01	-.58
LC9	.05	.46	.00	.00	.03	-.86	.05	.12	-.02	.00	.19
LC10	-.05	-.44	-.00	-.01	.00	-.23	.83	.11	-.09	.01	-.21
LC11	.04	.51	.00	.01	.15	.45	.47	.31	.07	.01	.44

In Table HEDL-7, the expression for LC1 is given by LC1 = -.06C + .00 Mn - .99P. . . .+ .02 and similarly for the other linear combinations. The elemental symbols represent the chemical concentration in weight per cent (not weight decimal fraction) and CN is the constant to be added. The embrittlement coefficients and variances are shown in Table HEDL-8. All off-diagonal covariances are zero.

From the information in Tables HEDL-7 and -8 it is possible to construct a formula similar to Eq (1), where the Charpy temperature shift is given by

$$\Delta(\text{NDTT}) = \text{LC1}^* (\text{LC1 Coeff. from Table HEDL-VII}) + \text{LC2}^* (\text{LC2 Coeff. from Table HEDL-VII}) + \text{etc.} \quad (2)$$

From Tables HEDL-7 and -8 we see that the Biemiller data has Ni, Cr, and Mn strongly entangled. This is much the same information that can be derived from a correlation matrix, but is a different way of displaying it.

TABLE HEDL-8

EMBRITTLEMENT COEFFICIENTS AND VARIANCES FOR DECOUPLED COMBINATIONS OF ELEMENTS, FOR AN IRRADIATION TO 3×10^{19} n/cm^2 (E>1.0 MeV)

Linear Combination	Charpy Shift Embrittlement Coeff. °C/(unit value of LC)	Variance
LC1	-.3994E + 04	.2912E + 07
LC2	-.8354E + 03	.2110E + 06
LC3	-.1225E + 02	.8833E + 05
LC4	-.6496E + 02	.3931E + 05
LC5	-.2686E + 03	.1010E + 05
LC6	-.4067E + 03	.3135E + 04
LC7	-.2319E + 02	.2474E + 04
LC8	-.3744E + 02	.1294E + 04
LC9	-.2938E + 02	.8981E + 02
LC10	-.5935E + 02	.3831E + 02
LC11	.4470E + 02	.6613E + 01

The covariance matrix of the coefficients of Case VIII is given in Table HEDL-9, using Mn, P, Ni, Cr, Mo, Cu, and V as relevant elements, and assuming that the best values of the coefficients are those shown for Case VIII in Table HEDL-4. The significance of the covariance matrix is that the square of the uncertainty in the temperature shift for a 3×10^{19} n/cm^2 (E>1.0 MeV) is given by

$$\overline{\Delta(\Delta(\mathrm{NDTT}))}^{\,2} = \sum_m \sum_n A_n C_{nm} A_m$$

In the formula above, $\overline{\Delta(\Delta(\mathrm{NDTT}))}^{\,2}$ is the square of the uncertainty

in the temperature shift, and A_1, A_2, etc., are the weight per cent concentrations of the chemical elements, C_{nm} are the mathematical elements in the covariance matrix, and the summation is taken over the adjustable coefficients including the additive constant. The "weight per cent," "A," for the constant term is to be taken as unity in applying the formula.

Table HEDL-10 shows a correlation matrix constructed for Case I of Table IV. From the correlation matrix it appears that the data are such that the coefficient for Mo is not independent of the coefficients for Cr, Ni, and Mn. This interdependence also shows in Table VII, which gives the particular linear combinations of elements that can be used to diagonalize the covariance matrix for Case I. None of the linear combinations shows Mo as a clearly dominant constituent. This phenomenon is due to correlations between Mo concentrations and other elemental concentrations in the available data.

For an irradiation to a fluence other than 3×10^{19} n/cm^2 (E>1.0 MeV), the formulas in this report can be used to predict the nil ductility shift as follows. (1) Use the coefficients of Case VIII together with the known chemistry of the specimen of interest to predict the nil ductility temperature shift at 3×10^{19} n/cm^2 (E>1.0 MeV). (2) Correct the previous value by multiplying by $(\emptyset t/3 \times 10^{19})^{0.43}$. where $\emptyset t$ is expressed in units of n/cm^2 (E>1.0 MeV).

TABLE HEDL-9

COVARIANCE MATRIX FOR SET OF EMBRITTLEMENT PARAMETERS FOR THE ELEMENT SET SHOWN, FOR THE BIEMILLER AND BYRNE DATA EXPRESSED IN ^{o}C AND WEIGHT PER CENT.

	Mn	P	Ni	Cr	Mo	Cu	V	Constant
Mn	.6167E+03	-.5350E+04	.9587E+02	-.4352E+02	.6162E+03	-.1026E+02	-.5828E+03	-.1117E+04
P		.1787E+07	.1362E+04	-.2022E+04	.1999E+05	-.1096E+05	-.8562E+05	-.2094E+05
Ni			.1036E+03	-.4730E+02	.2305E+03	-.1693E+03	-.1265E+03	-.3040E+03
Cr				.2917E+03	-.1118E+04	.6330E+02	-.2875E+03	.5881E+03
Mo					.5784E+04	.3536E+03	-.7766E+04	-.3853E+04
Cu						.3004E+04	.1574E+03	-.4897E+03
V							.1744E+06	.3440E+04
Constant								.3864E+04

TABLE HEDL-10

CORRELATION MATRIX FOR THE EMBRITTLEMENT PARAMETERS FOR THE FULL SET OF TEN ELEMENTS PLUS AN ADDITIVE CONSTANT; CASE I, USING DATA OF BIEMILLER AND BYRNE

	C	Mn	P	S	Si	Ni	Cr	Mo	Cu	V	CNST.
C	1.00	.30	.43	-.05	.37	.55	.40	.05.	-.11	-.36	-.66
Mn	.30	1.00	-.03	.07	.11	.46	.05	.30	-.04	.13	-.69
P	.43	-.03	1.00	-.38	.08	.32	.09	.23	-.18	-.35	-.43
S	-.05	.07	-.38	1.00	.01	-.06	.11	-.18	.01	.28	.08
Si	.37	.11	.08	.01	1.00	.13	-.18	.22	.02	-.18	-.45
Ni	.55	.46	.32	-.06	.13	1.00	.05	.25	-.32	-.22	-.63
Cr	.40	.05	.09	.11	-.18	.05	1.00	-.77	-.02	-.12	.16
Mo	.05	.30	.23	-.18	.22	.25	-.77	1.00	.09	-.29	-.65
Cu	-.11	-.04	-.18	.01	.02	-.32	-.02	.09	-1.00	.04	-.04
V	-.36	-.13	-.36	.28	-.18	-.22	-.12	-.29	.04	1.00	.34
CNST.	-.66	-.69	-.43	.08	-.45	-.63	.16	-.65	-.04	.34	1.00

Expected Accomplishments in the next reporting period

At some time in the future additional data will be analyzed and the expression for the shift in nil ductility temperature will be enlarged to include terms involving products of concentrations of elements, as well as concentrations to the first power.

References and Footnotes

1. G. L. Guthrie and F. M. Bolting, "The Effect of Minor Elements on the Irradiation Sensitivity of Weld Metal," --LWR Pressure Vessel Irradiation Surveillance Dosimetry Quarterly Progress Report, October-December 1977, HEDL-TME 78-5, Hanford Engineering Development Laboratory, Richland, WA.

2. E. C. Biemiller and S. J. Byrne, "Evaluation of the Effect of Chemical Composition on the Irradiation Sensitivity of Reactor Vessel Weld Metal," ASTM STP 611, pp 418-433, American Society for Testing and Materials, (1976).

3. Due to an error in the computer program, in the previous report, the correction from degrees Fahrenheit to degrees centigrade was performed twice, so the resulting coefficients are reported as 5/9 of their true value.

4. Regulatory Guide 1.99, U. S. Nuclear Regulatory Commission.

5. B. R. Martin, Statistics for Physicists, Academic Press, New York, N. Y. 1971, pp 85-94.

6. William Mendenhall and Richard L. Schaeffer, Mathematical Statistics with Applications, pp 410-416, Duxbury Press, North Scituate, Massachusetts (1973).

Oak Ridge National Laboratory (ORNL)

A. POOL CRITICAL ASSEMBLY PRESSURE VESSEL WALL BENCHMARK FACILITY (PCA-PVF)

J. H. Swanks
L. P. Pugh

Objective

To design, fabricate, install, checkout, and operate the PCA-PVF.

Summary

Design, fabrication, and preparation are continuing to prepare the PCA-PVF for dosimetry experiments.

Accomplishments and Status

Design work performed this quarter for the Pool Critical Assembly (PCA) facility has been to accommodate changes and/or additions requested by experimenters. Included are designs of free-field measurement facilities, Lucite follower plugs for experiment tubes, a fission chamber tube for run-to-run normalization, a lead thermal shield, and core mapping rigs. Analyses and documentation of the adequacy of the structural capabilities of the PCA experiment facility with the stainless steel thermal shield and of the BSR pool floor were completed by General Engineering.

Fabrication of most of the major facility components has been completed during this reporting period. The pressure vessel simulator and dosimetry capsule were procured rough cut from the steel supplier to save considerable time and machining costs.

Preparation of the PCA for the experiment program was begun this quarter. The core and control rods were moved two rows southward to position them in their most southward position (thus, adjacent to the

aluminum window simulator of the experiment rig). Additional end box adapters were fabricated to provide flexibility in loading Pool Critical Assembly (PCA), Bulk Shielding Reactor (BSR), and Oak Ridge Research Reactor (ORR) core components in any core position. Gamma dose rates were measured in water as a function of distance from the reactor face to assist experimenters in planning for their measurements. A number of possible core configurations were assembled to determine their suitability for the experiment program. Core number 238 (Figure ORNL-1) was most desirable. It provides four-quadrant symmetry with the rods withdrawn approximately nineteen inches. The Experiment Review Questionnaire has been completed and approved.

The Quality Assurance Program Plan (QAPP) has been completed and approved by Oak Ridge National Laboratory (ORNL) management.

Expected Accomplishments

The fabrication, installation, and checkout of the PCA-PVF will be completed by the end of the current reporting period. The facility will then be ready for dosimetry experiments.

POOL CRITICAL ASSEMBLY
Core Loading No. 238

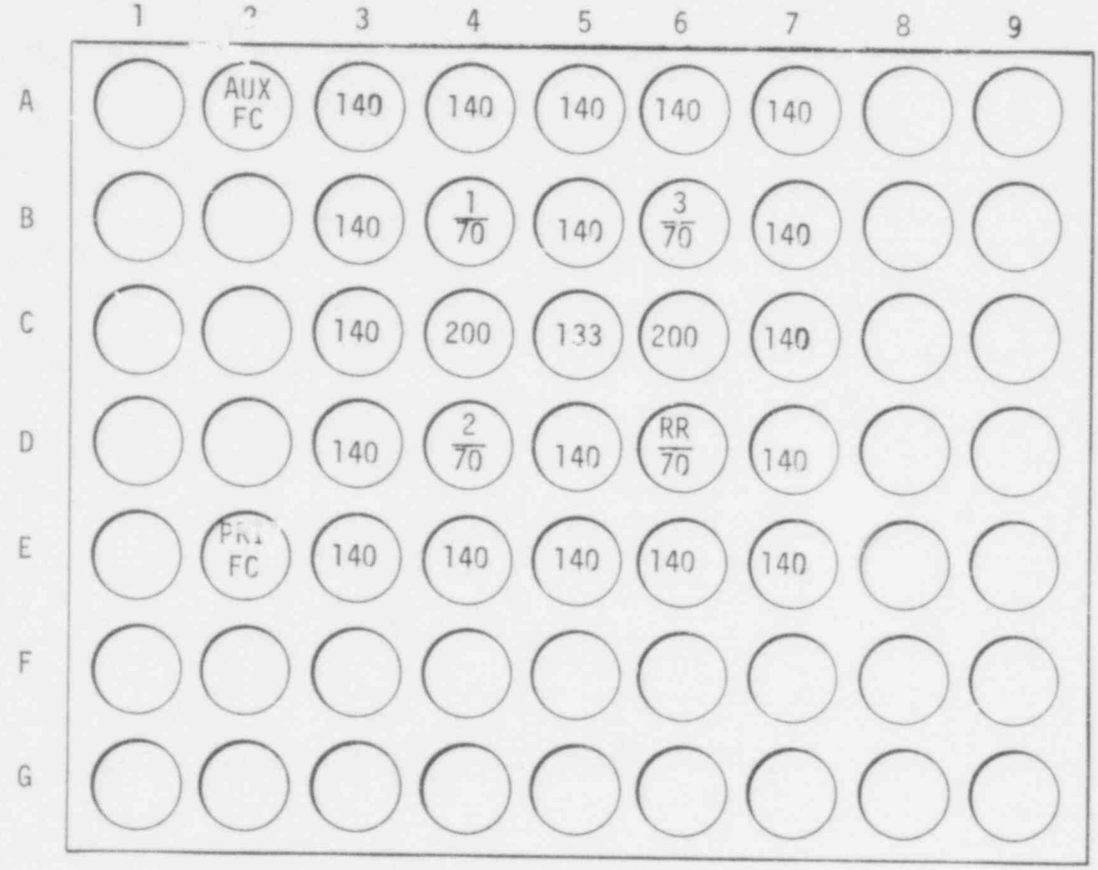

CRITICAL MASS: 3,336.010

ROD POSITIONS: No. 1 Safety: 19
No. 2 Safety: 19
No. 3 Safety: 19
Regulating Rod: 15.13

FIGURE ORNL-1. Pool Critical Assembly Core Loading No. 238

B. OAK RIDGE RESEARCH REACTOR PRESSURE VESSEL WALL BENCHMARK FACILITY (ORR-PVF)

J. H. Swanks
L. P. Pugh

Objective

To design, fabricate, install, and check out the ORR-PVF.

Summary

Assembly, layout work, and detailed design of the ORR experiment facility are 85% complete. Engineering drawings are ready to be checked.

Accomplishments and Status

Assembly and layout work and detailed design of the ORR experiment facility are 85% complete. The engineering drawings are ready to be checked. The major component still to be designed is the drive mechanism for the pressure vessel simulator. Evaluation of possible concepts is progressing. General Engineering has completed and documented their structural and thermal analyses of the experiment facility. Structural capabilities of the window shelf are adequate to support the experiment structure.

The Quality Assurance Program Plan (QAPP) has been completed and approved by Oak Ridge National Laboratory (ORNL) management.

Expected Accomplishments

The assembly, layout work, and detailed design of the ORR experiment facility will be completed by the end of the next reporting period. The engineering drawings will be checked and fabrication initiated.

C. DESIGN SUPPORT CALCULATIONS

L. F. Miller
F. B. K. Kam

Objective

Additional design support neutron transport calculations have been performed in order to evaluate two design alternatives:

1. sandwiching the test specimens between copper plates; and
2. placing a set of test specimens directly behind the thermal shield.

Summary

Changes in spatial and spectral characteristics of the neutron flux in the pressure vessel simulator are relatively small; consequently, these two design alternatives are considered admissible. The results and analysis of these calculations (cases 10 through 12) are presented herein.

Accomplishments and Status

Most of the design support calculations have been reported in previous quarterly reports. In particular, the two-dimensional calculations were reported in the October through December 1977 quarterly report, and nine one-dimensional calculations (cases 1 through 9) were reported in the January through March 1978 quarterly report. Three additional one-dimensional calculations (cases 10 through 12) are reported herein, and cross-section sets are being prepared for two additional one-dimensional calculations (cases 13 through 14).

An illustration of the composition and geometry of the reference case (case 1) one-dimensional calculation is given in Figure ORNL-1. The

group structure for all cases is given in Table ORNL-1. Results pertaining to placing one-eighth inch copper plates on each side of the three sets of test specimens (cases 10 and 11) are given in Tables ORNL-2-5. The effect of placing a row of test specimens immediately behind the thermal shield (a comparison between cases 1 and 12) is illustrated in Tables ORNL-6 and -7. A description of the geometry for cases 10, 11, and 12 is given in Tables ORNL-8-10.

Cases 10 and 11 have the same mesh interval specification; this allows for placing an arbitrary material, one-eighth inch thick, on each side of the three sets of test specimens. Case 10 is the reference calculation with iron for the entire pressure vessel simulator, and case 11 includes the six copper regions specified. Spectra for these two cases, at three locations, are given in Tables ORNL-2-4. Most of the group fluxes change very little; however, one changes by seven per cent. On the other hand, it may be noted from Table ORNL-5 that maximum change in the fast flux is about two per cent. Since fast flux is closely related to the function of interest (i.e., the damage function), it is concluded that the inclusion of the six copper plates is acceptable from a neutronics point of view. Also, it is expected that the plates will be one-sixteenth of an inch thick rather than one-eighth inch since the one-sixteenth inch plate provides for adequate temperature flattening.

It is expected that a set of test specimens will be placed directly behind the thermal shield. Case 12 differs from case 1 by making the thermal shield 3.81 cm thicker (i.e., 9.81 cm thick) and replacing 3.81 cm of water between the thermal shield and pressure vessel simulator (c.f. Table ORNL-10). It may be noted from Table ORNL-6 that the spectral differences between cases 1 and 12 are significant. However, the differences in the fast flux, given by Table ORNL-7, at several locations in the pressure vessel simulator, are less than two per cent. Smaller spectral changes would be observed if iron replaces water in front of the thermal shield. This conclusion is supported by comparison of cases 1 and 4. Although the spectral effect is significant and is of some concern, an integral

quantity of interest, the fast flux, does not change significantly. Thus, this change is also considered acceptable from neutronic considerations.

Expected Accomplishments

Two additional calculations are in progress:

1. to determine the effect of replacing the thermal shield with lead; and
2. to evaluate the effect of poisoning the core with boron to achieve a critical system.

Replacement of the thermal shield with lead will reduce the gamma-to-neutron ratio (γ/n); a smaller γ/n ratio is needed to make spectral measurements beyond the thermal shield in the Pool Critical Assembly (PCA) experiment. Poisoning the core will provide information on the importance of thermal self shielding and fission products in the core model.

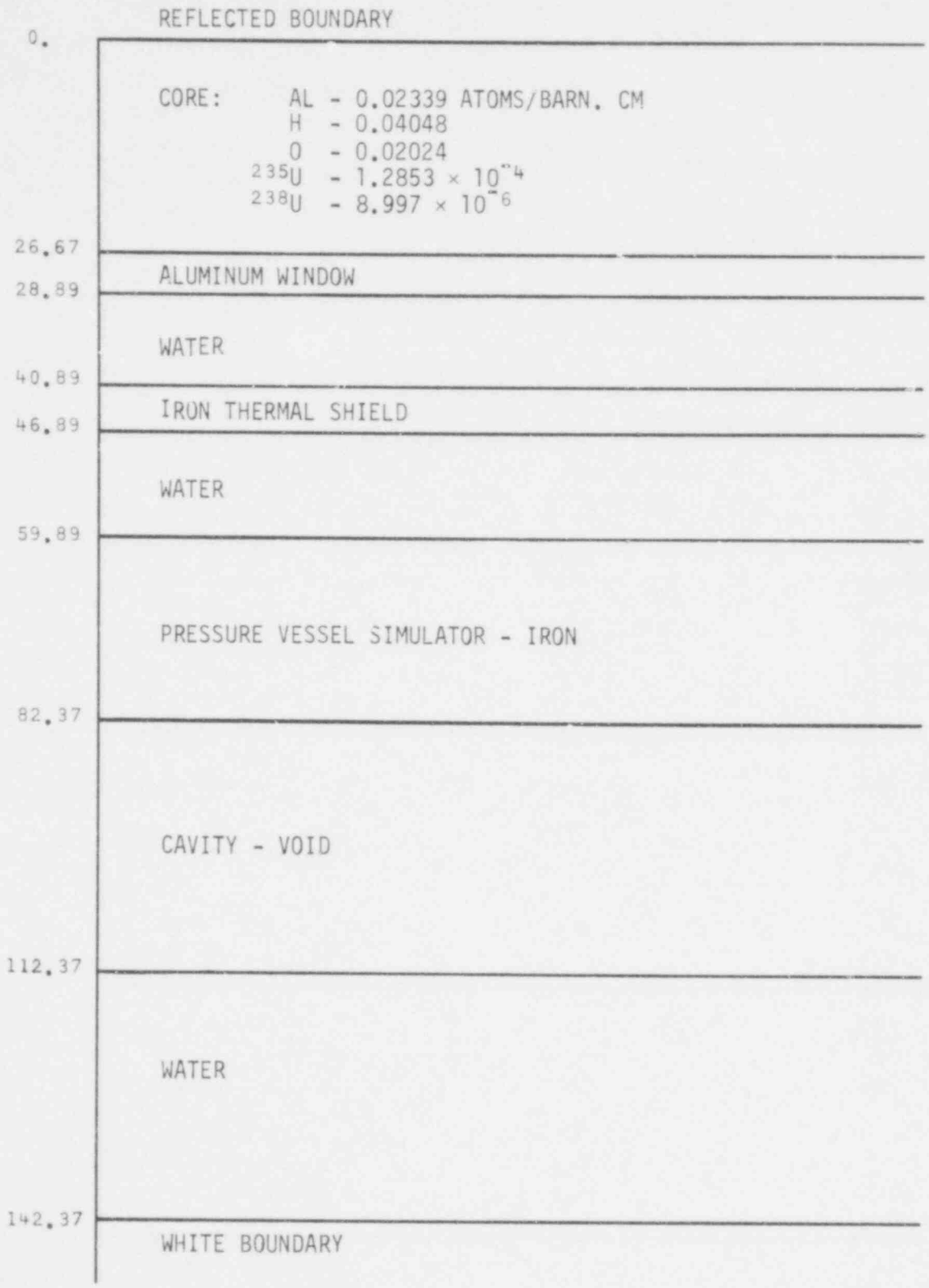

FIGURE ORNL-2. Reference Case for 1-D Neutron Design Calculations

TABLE ORNL-1

Energy and Lethargy Boundaries for Following Spectra Tables

Group Number (i)	Lower Lethargy Boundary (Ui)	ΔU_i	Upper Energy Boundary (eV)
1	-6.93147 E-1	1.134135	2.000 E+7
2	4.40988 E-1	0.292981	6.434 E+6
3	7.33969 E-1	0.470001	4.800 E+6
4	1.20397	0.2425	3.000 E+6
5	1.44647	0.55158	2.354 E+6
6	1.99805	0.50299	1.356 E+6
7	2.50104	0.49565	8.200 E+5
8	2.99669	0.41456	4.9952 E+5
9	3.41125	0.78846	3.300 E+5
10	4.19971	0.40546	1.500 E+5
11	4.60517	1.44022	1.000 E+5
12	6.04539	5.26871	1.300 E+4
13	1.13141 E+1	4.1834	1.220 E+2
14	1.54975 E+1	1.2184	1.860 E+0
15	1.67159 E+1	10.9151	5.500 E-1
	2.76310 E+1		1.000 E-5

TABLE ORNL-2

Comparison of Spectra from a Reference Calculation (Case 10) and a Calculation with the Test Specimens Sandwiched Between Copper Plates (Case 11): the Location is at the First Plate Midpoint (interval 52, r = 59.7337)

Group Number (i)	$\phi_i \Delta U_i$		$\sum_{i=1}^{N} \phi_i \Delta U_i$		Ratio of Group Fluxes Case 10/Case 11
	Case 10	Case 11	Case 10	Case 11	
1	5.666 E-5	5.657 E-5	5.666 E-5	5.657 E-5	1.001
2	4.564 E-5	4.528 E-5	1.023 E-4	1.018 E-4	1.007
3	8.154 E-5	7.994 E-5	1.838 E-4	1.818 E-4	1.020
4	7.059 E-5	6.852 E-5	2.544 E-4	2.503 E-4	1.030
5	1.561 E-4	1.509 E-4	4.105 E-4	4.012 E-4	1.034
6	1.391 E-4	1.396 E-4	5.497 E-4	5.408 E-4	0.9964
7	1.597 E-4	1.614 E-4	7.094 E-4	7.022 E-4	0.9894
8	1.025 E-4	1.038 E-4	8.118 E-4	8.060 E-4	0.9874
9	1.571 E-4	1.605 E-4	9.689 E-4	9.665 E-4	0.9788
10	6.166 E-5	6.222 E-5	1.031 E-3	1.029 E-3	0.9909
11	2.058 E-4	1.951 E-4	1.236 E-3	1.224 E-3	1.054
12	3.131 E-4	2.945 E-4	1.549 E-3	1.518 E-3	1.063
13	2.864 E-4	2.772 E-4	1.836 E-3	1.796 E-3	1.033
14	8.475 E-5	8.164 E-5	1.921 E-3	1.877 E-3	1.038
15	1.300 E-3	1.114 E-3	3.220 E-3	3.021 E-3	1.136

TABLE ORNL-3

Comparison of Spectra from a Reference Calculation (Case 10) and a Calculation with the Test Specimens Sandwiched Between Copper Plates (Case 11): the Location is at the Third Plate Midpoint (interval 60, r = 64.337 cm)

Group Number (i)	$\phi_i \Delta U_i$		$\sum_{i=1}^{N} \phi_i \Delta U_i$		Ratio of Group Fluxes Case 10/Case 11
	Case 10	Case 11	Case 10	Case 11	
1	2.400 E-5	2.377 E-5	2.400 E-5	2.377 E-5	1.009
2	1.966 E-5	1.935 E-5	4.367 E-5	4.313 E-5	1.016
3	3.839 E-5	3.715 E-5	8.206 E-5	8.027 E-5	1.033
4	3.806 E-5	3.629 E-5	1.201 E-4	1.166 E-4	1.048
5	1.080 E-4	1.022 E-4	2.281 E-4	2.188 E-4	1.056
6	1.291 E-4	1.272 E-4	3.572 E-4	3.460 E-4	1.014
7	1.815 E-4	1.823 E-4	5.387 E-4	5.282 E-4	0.9956
8	1.334 E-4	1.337 E-4	6.720 E-4	6.619 E-4	0.9977
9	2.020 E-4	2.074 E-4	8.740 E-4	8.693 E-4	0.9739
10	8.119 E-5	8.228 E-5	9.552 E-4	9.516 E-4	0.9867
11	2.786 E-4	2.393 E-4	1.234 E-3	1.191 E-3	1.164
12	1.812 E-4	1.569 E-4	1.415 E-3	1.348 E-3	1.154
13	1.504 E-4	1.391 E-4	1.565 E-3	1.487 E-3	1.081
14	2.582 E-5	2.373 E-5	1.591 E-3	1.511 E-3	1.088
15	5.798 E-5	4.714 E-5	1.649 E-3	1.558 E-3	1.229

TABLE ORNL-4

Comparison of Spectra from a Reference Calculation (Case 10) and a Calculation with the Test Specimens Sandwiched Between Copper Plates (Case 11): the Location is at the Third Plate Midpoint (interval 70, r = 69.9572 cm)

Group Number (i)	$\phi_i \Delta U_i$		$\sum_{i=1}^{N} \phi_i \Delta U_i$		Ratio of Group Fluxes Case 10/Case 11
	Case 10	Case 11	Case 10	Case 11	
1	8.383 E-6	8.243 E-6	8.383 E-6	8.243 E-6	1.017
2	6.704 E-6	6.550 E-6	1.509 E-5	1.479 E-5	1.023
3	1.401 E-5	1.344 E-5	2.910 E-5	2.823 E-5	1.042
4	1.512 E-5	1.427 E-5	4.422 E-5	4.250 E-5	1.059
5	5.222 E-5	4.879 E-5	9.644 E-5	9.129 E-5	1.070
6	8.269 E-5	8.009 E-5	1.791 E-4	1.714 E-4	1.032
7	1.423 E-4	1.409 E-4	3.214 E-4	3.123 E-4	1.009
8	1.170 E-4	1.152 E-4	4.384 E-4	4.275 E-4	1.015
9	1.856 E-4	1.884 E-4	6.241 E-4	6.159 E-4	0.9851
10	7.724 E-5	7.760 E-5	7.013 E-4	6.935 E-4	0.9953
11	2.768 E-4	2.315 E-4	9.781 E-4	9.250 E-4	1.195
12	1.088 E-4	9.368 E-5	1.087 E-3	1.019 E-3	1.161
13	7.672 E-5	6.781 E-5	1.164 E-3	1.086 E-3	1.131
14	9.913 E-6	8.611 E-6	1.174 E-3	1.095 E-3	1.151
15	3.054 E-6	2.339 E-6	1.177 E-3	1.097 E-3	1.305

TABLE ORNL-5

Fast Flux,[a] Total Flux,[b] and Fast Flux Normalized to the Pressure Vessel Surface at Selected Penetration Distances into the Pressure Vessel Simulator: Case 10 is the Reference Calculation and Case 11 has Copper Plates on Each Side of the Test Specimens

Interval Number	Penetration Distance	Distance From Center Line	Fast Flux	
			Case 10	Case 11
52	0.1587	59.733	1.031 E-3	1.029 E-3
60	4.7625	64.337	9.552 E-4	9.516 E-4
70	10.382	69.957	7.013 E-4	6.935 E-4

Total Flux		Interval Number	Normalized Fast Flux	
Case 10	Case 11		Case 10	Case 11
3.220 E-3	3.021 E-3	52	1.0	1.0
1.649 E-3	1.558 E-3	60	0.9264	0.9247
1.177 E-3	1.097 E-3	70	0.6802	0.6739

[a] $\left(\sum_{i=1}^{10} \phi_i \Delta U_i \right)$

[b] $\left(\sum_{i=1}^{15} \phi_i \Delta U_i \right)$

TABLE ORNL-6

Comparison of Spectra from a Reference Calculation (Case 1) and a Calculation With Test Specimens Directly Behind the Thermal Shield (Case 12): the Location is at 1/4-T (interval 61, 6.369 cm penetration into vessel)

Group Number (i)	$\phi_i \Delta U_i / \Delta U_i$ (Normalized)		$\sum_{i=1}^{i} \phi_i \Delta U_i$ (Unnormalized)		Ratio of Group Fluxes Case 1/Case 12
	Case 1	Case 12	Case 1	Case 12	
1	1.079 E-2	6.591 E-3	1.726 E-5	1.217 E-5	1.418
2	3.384 E-2	2.170 E-2	3.124 E-5	2.252 E-5	1.350
3	4.185 E-2	2.945 E-2	5.897 E-5	4.505 E-5	1.230
4	8.226 E-2	6.202 E-2	8.715 E-5	6.954 E-5	1.150
5	1.091 E-1	8.971 E-2	1.720 E-4	1.501 E-4	1.054
6	1.555 E-1	1.378 E-1	2.823 E-4	2.629 E-4	0.9778
7	2.351 E-1	2.219 E-1	4.467 E-4	4.420 E-4	0.9184
8	2.140 E-1	2.034 E-1	5.720 E-4	5.793 E-4	0.9126
9	1.725 E-1	1.682 E-1	7.636 E-4	7.950 E-4	0.8878
10	1.362 E-1	1.348 E-1	8.414 E-4	8.840 E-4	0.8738
11	9.382 E-2	1.366 E-1	1.111 E-3	1.204 E-3	0.8429
12	2.208 E-2	2.319 E-2	1.257 E-3	1.403 E-3	0.7310
13	1.956 E-2	2.479 E-2	1.372 E-3	1.572 E-3	0.682
14	1.028 E-2	1.335 E-2	1.390 E-3	1.599 E-3	0.6666
15	1.311 E-3	1.679 E-3	1.432 E-2	1.628 E-3	0.6766

TABLE ORNL-7

Fast Flux,[a] Total Flux,[b] and Fast Flux Normalized to the Pressure Vessel Surface at Selected Penetration Distances into the Pressure Vessel: Results are for a Reference Calculation (Case 1) and for a Calculation with Test Specimens Directly Behind the Thermal Shield (Case 12)

Interval Number	Penetration Distance	Distance From Center Line	Fast Flux	
			Case 1	Case 12
53	0.3746	60.2671	9.896 E-4	1.051 E-3
61	6.369	66.2615	8.414 E-4	8.840 E-4
68	11.6141	71.5066	6.092 E-4	6.358 E-4

Total Flux		Interval	Normalized Fast Flux	
Case 1	Case 12	Number	Case 1	Case 12
2.867 E-3	3.800 E-3	53	1.0	1.0
1.410 E-3	1.628 E-3	61	0.8502	0.8411
1.023 E-3	1.139 E-3	68	0.6156	0.6049

[a] $\left(\sum_{i=1}^{10} \phi_i \Delta U_i \right)$

[b] $\left(\sum_{i=1}^{15} \phi_i \Delta U_i \right)$

TABLE ORNL-8

Case Number 1C
One-Dimensional XSDRN Calculations

Zone	Zone Description	Material	Atm/B-cm Density	Radii	Width
I	Core	H	4.048 E-2	0.0	26.67
		O	2.024 E-2		
		Al	2.339 E-2		
		^{235}U	1.285 E-3		
		^{238}U	8.997 E-6		
Ii	Aluminum Widnow	Al	6.030 E-2	26.67	2.225
III	Primary Window Coolant	H	6.680 E-2	28.8925	12.00
			3.340 E-2		
IV	Thermal Shield	Fe	8.480 E-2	40.8925	6.
		C			
		Mn			
		Si			
		Cr			
		Ni			
V	Primary Water Coolant	H	6.680 E-2	46.8925	12.6825
		O			
VI	Copper Plate (position)	Fe	8.480 E-2	59.5750	0.3175
VII	Test Specimen	Fe	8.480 E-2	59.8925	2.032
VIII	Copper Plate (position)	Fe	8.480 E-2	61.9245	0.3175
IX	Pressure Vessel	Fe	8.480 E-2	62.2420	1.9367
X	Copper Plate (position)	Fe	8.480 E-2	64.1787	0.3175
XI	Test Specimen	Fe	8.480 E-2	64.4962	2.032
XII	Copper Plate (position)	Fe	8.480 E-2	66.5282	0.3175
XIII	Pressure Vessel	Fe	8.480 E-2	66.8457	2.9528
XIV	Copper Plate (position)	Fe	8.480 E-2	69.7985	0.3175
XV	Test Specimen	Fe	8.480 E-2	70.1160	2.032
XVI	Copper Plate (position)	Fe	8.480 E-2	72.1480	0.3175
XVII	Pressure Vessel	Fe	8.480 E-2	72.4655	9.906
XVIII	Cavity	Void	1.000 E-10	82.3715	30.
XIX	Water	H	6.68 E-2	112.371	30.
		O	3.34 E-2		

TABLE ORNL-9

Case Number 11
One-Dimensional XSDRN Calculations

Zone	Zone Description	Material	Atm/B-cm Density	Radii	Width
I	Core	H	4.048 E-2	0.0	26.67
		O	2.024 E-2		
		Al	2.339 E-2		
		^{235}U	1.285 E-3		
		^{238}U	8.997 E-6		
II	Aluminum Window	Al	6.030 E-2	26.67	2.225
III	Primary Water Coolant	H	6.680 E-2	28.8925	12.00
		O	3.340 E-2		
IV	Thermal Shield	Fe	8.480 E-2	40.8925	6.
		C			
		Mn			
		Si			
		Cr			
		Ni			
V	Primary Water Coolant	H	6.680 E-2	46.8925	12.6825
		O			
VI	Copper Plate	Cu	8.493 E-2	59.575	0.3175
VII	Test Specimen	Fe	8.480 E-2	59.892	2.032
VIII	Copper Plate	Cu	8.493 E-2	61.9245	0.317
IX	Pressure Vessel	Fe	8.480 E-2	62.2420	1.9367
X	Copper Plate	Cu	8.493 E-2	64.1787	0.3175
XI	Test Specimen	Fe	8.480 E-2	64.4962	2.032
XII	Copper Plate	Cu	8.493 E-2	66.5282	0.3175
XIII	Pressure Vessel	Fe	8.480 E-2	66.8457	2.9528
XIV	Copper Plate	Cu	8.493 E-2	69.7985	0.3175
XV	Test Specimen	Fe	8.480 E-2	70.1160	2.032
XVI	Copper Plate	Cu	8.493 E-2	72.1480	0.3175
XVII	Pressure Vessel	Fe	8.480 E-2	72.4655	9.906
XVIII	Cavity	Void	1.000 E-10	82.3715	30.
XIX	Water	H	6.68 E-2	112.371	30.
		O	3.34 E-2		

TABLE ORNL-10

Case Number 12
One-Dimensional XSDRN Calculations

Zone	Zone Description	Material	Atm/B-cm Density	Radii	Width
I	Core	H	4.048 E-2	0.0	26.67
		O	2.024 E-2		
		Al	2.339 E-2		
		^{235}U	1.2853 E-4		
		^{238}U	8.997 E-6		
II	Aluminum Window	Al	6.030 E-2	26.67	2.2225
III	Primary Water Coolant	H	6.680 E-2	28.8925	12.00
		O	3.340 E-2		
IV	Thermal Shield	Fe	8.480 E-2	40.8925	9.81
		C			
		Mn			
		Si			
		Cr			
		Ni			
V	Primary Water Coolant	H	6.680 E-2	50.7025	9.19
		O	3.340 E-2		
VI	Pressure Vessel	Fe	8.480 E-2	59.8925	22.479
VII	Cavity	Void	1.000 E-10	82.3715	30.00
VIII	Water	H	6.680 E-2	112.3715	30.00
		O	3.340 E-2		
				142.3715	

D. INSTRUMENTED IRRADIATION CAPSULE (IIC)

J. A. Conlin
I. Siman-Tov

Objective

To design, fabricate, install, checkout, and maintain the IIC.

Summary

The drawings of the capsule representing the pressure vessel are about 50% complete. A two-dimensional heat transfer model of the entire pressure vessel capsule has been developed. A two-dimensional model of the surveillance specimen capsule was also developed. The detailed design of the pressure vessel capsule containment is nearing completion. The heater plate design has been modified.

Accomplishments and Status

Introduction

The pressure vessel steel Oak Ridge Research Reactor (ORR) capsule is designed to provide a direct comparison of the radiation damage to Pressurized Water Reactor (PWR) pressure vessel surveillance specimens to that of the actual pressure vessel. PWRs contain surveillance specimens located between the stainless steel thermal shield and the pressure vessel.

This irradiation experiment consists of two capsules. One, the Surveillance Specimen Capsule (SSC), represents the surveillance specimens of a PWR and the other, the pressure vessel capsule (PVC), the reactor pressure vessel. The experiment is to be irradiated in the ORR poolside

facility. The facility will contain a mockup of a thermal shield 27" × 27" × 6 cm thick and an 8.85 in. thick section of steel representing the pressure vessel. Behind the simulated pressure vessel will be an air-filled-aluminum box representing the void on the outside of a PWR vessel. The surveillance specimen capsule will be mounted on the "outer" face of the thermal shield and the pressure vessel capsule in a "U" shaped cut out in the steel representing the pressure vessel. The surveillance capsule will contain one region of charpie and compact tensile specimens. The pressure vessel capsule will contain a similar set of specimens at three regions; the inner face, at the 1/4 thickness and at the 1/2 thickness positions. Temperatures of all specimens are to be maintained at 283°C ±10°C (550°F).

Capsule Design

The basic capsule design for the PVC remains the same as that described in the previous quarterly report. The drawings of the capsule representing the pressure vessel are about 50% complete. Some minor modifications have been made. The actual location of the specimens relative to the ORR core has been changed to increase the exposure dose. This has required a new gamma heating calculation which models the new position of the thermal shield, surveillance specimen capsule (SSC) and instrumented pressure vessel capsule (PVC). These are one-dimensional calculations and do not adequately model the effect of the surveillance specimen capsule (SSC) since its dimensions are small enough to allow some three-dimensional effects on the gamma heat. For this reason, two cases will be run; one with and one without the surveillance specimen capsule to obtain the range of effect that the SSC could have on the gamma heating in the PVC. The case with the SSC in place has been run; the other is in progress. The results may require some minor modifications to the thermal design, in particular the sizing of gas gaps.

A two-dimensional heat transfer model (Model V) of the entire PVC has been developed (Figure ORNL-3). This model represents the entire capsule in XZ geometry. (The model represents a capsule of infinite size in the

horizontal direction parallel to the ORR window, Y direction.) This model maps the heat flows between the three specimen regions and will establish the final sizing of insulating gas gaps and electric heater loads necessary to maintain the design temperature.

A two-dimensional model (XZ geometry) of the surveillance specimen capsule (Figure ORNL-4) was also developed using the newly-calculated gamma heating rates and will be used to finalize the design of that capsule.

The SSC will consist of a single test specimen assembly clamped in a steel frame sandwiched between two heater plate assemblies identical to that of the PVC. There are to be no cooler plates since the capsule is small enough such that internal cooling will not be required. The specimen-heater assembly will be contained in a stainless steel box with a 1/4 in. gas gap on top, bottom, and both sides. The front and back will be of 0.09 in. thick stainless plates through which the heat will be transmitted to pool water. There will be a thermal barrier between the specimen-heater assembly and the front and back surfaces of the box. This may be a gas gap similar to that of the PVC, or another form of thermal barrier may be required. The heat flux through these surfaces is greater than in the PVC capsule and will require a smaller gas gap. Too small a gap may be difficult to maintain with sufficient accuracy for proper temperature control over the large 15" × 15" surface.

The detailed design of the PVC containment is nearing completion. We plan to build a prototype to verify assembly techniques and to provide a test vessel in which to evaluate the performance of prototype heater and cooler plate assemblies.

A prototype cooler plate assembly was machined; however, improper machining techniques resulted in nonuniform gas gaps surrounding the cooler tubes. A new cooler plate is to be fabricated. No real problems are anticipated.

The heater plate design has been modified. Previously, the heater plate was to be a brazed assembly with the heaters in grooves in one steel plate with a second plate covering the heaters and the entire assembly brazed. A test braze assembly indicated a need for some brazing development work if a satisfactory assembly were to be had. The design has been changed to avoid the need for brazing. The 1/16 in. sheathed heaters will be placed in grooves and a copper strip driven in to lock the heater in place and to ensure good heat transfer between the heater and steel plate. This assembly technique has been satisfactorily demonstrated. The groove and heater wire patterns are illustrated in Figure ORNL-3. These patterns are designed to minimize temperature edge effects due to the somewhat lower gamma heat at the edges and the heat losses from the capsule sides.

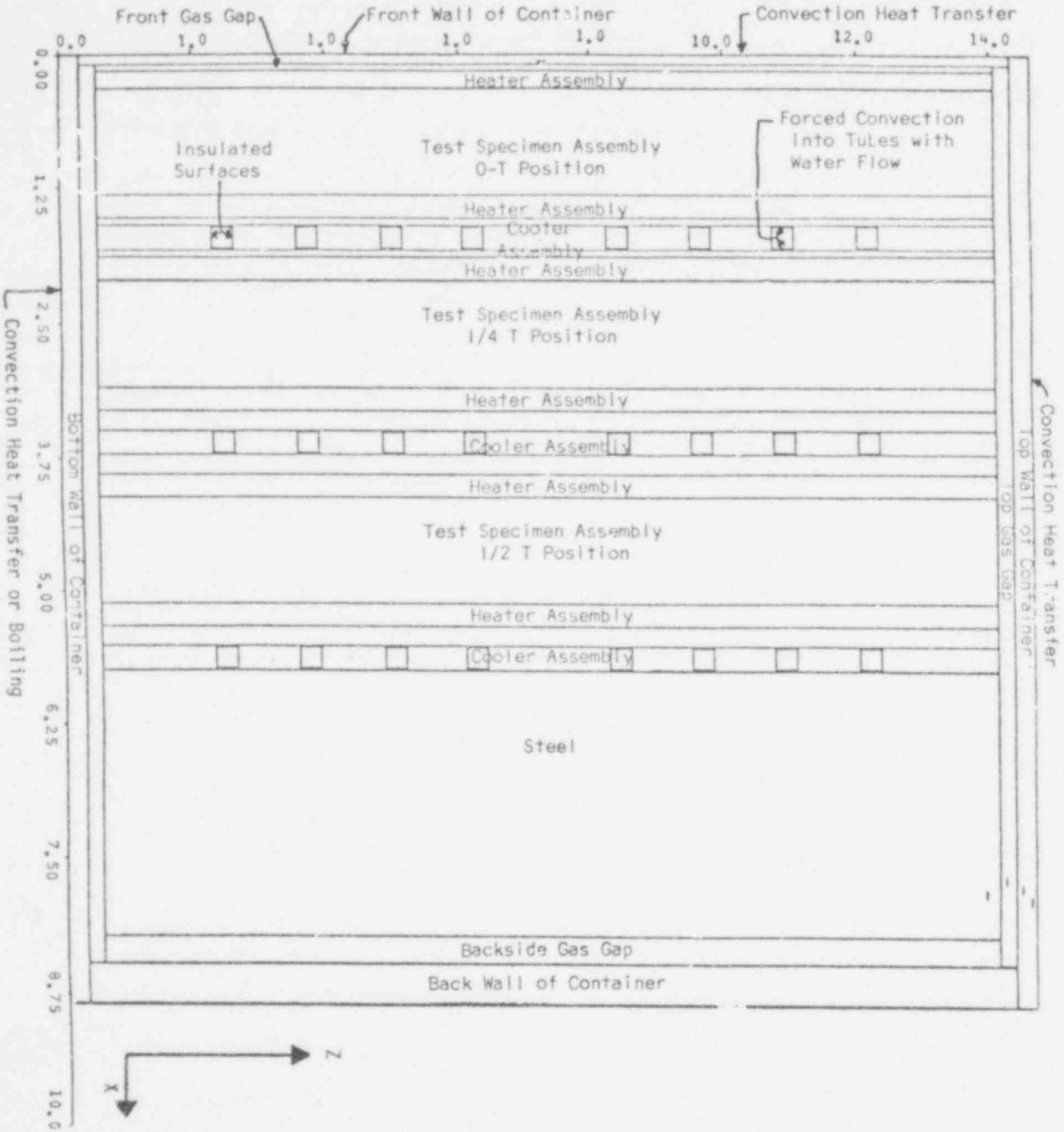

FIGURE ORNL-3. Model V Two-Dimensional XZ (XZ axes do not have the same scaling factor) Geometric Representation of the Instrumented Irradiation Capsule.

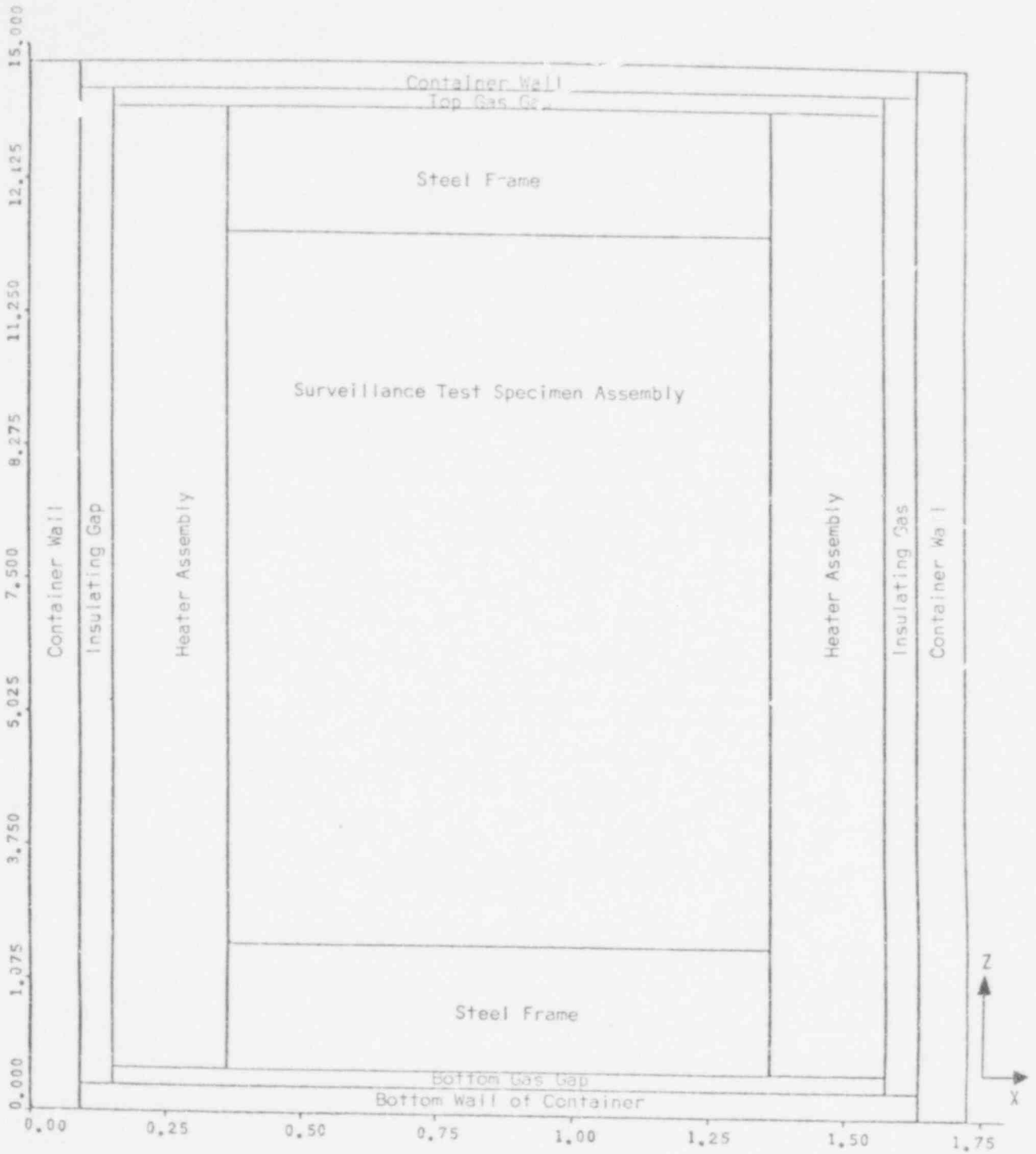

FIGURE ORNL-4. Surveillance Specimen Capsule Model SSC-1 Two-Dimensional XZ (X and Z do not have the same scaling factor) Geometry.

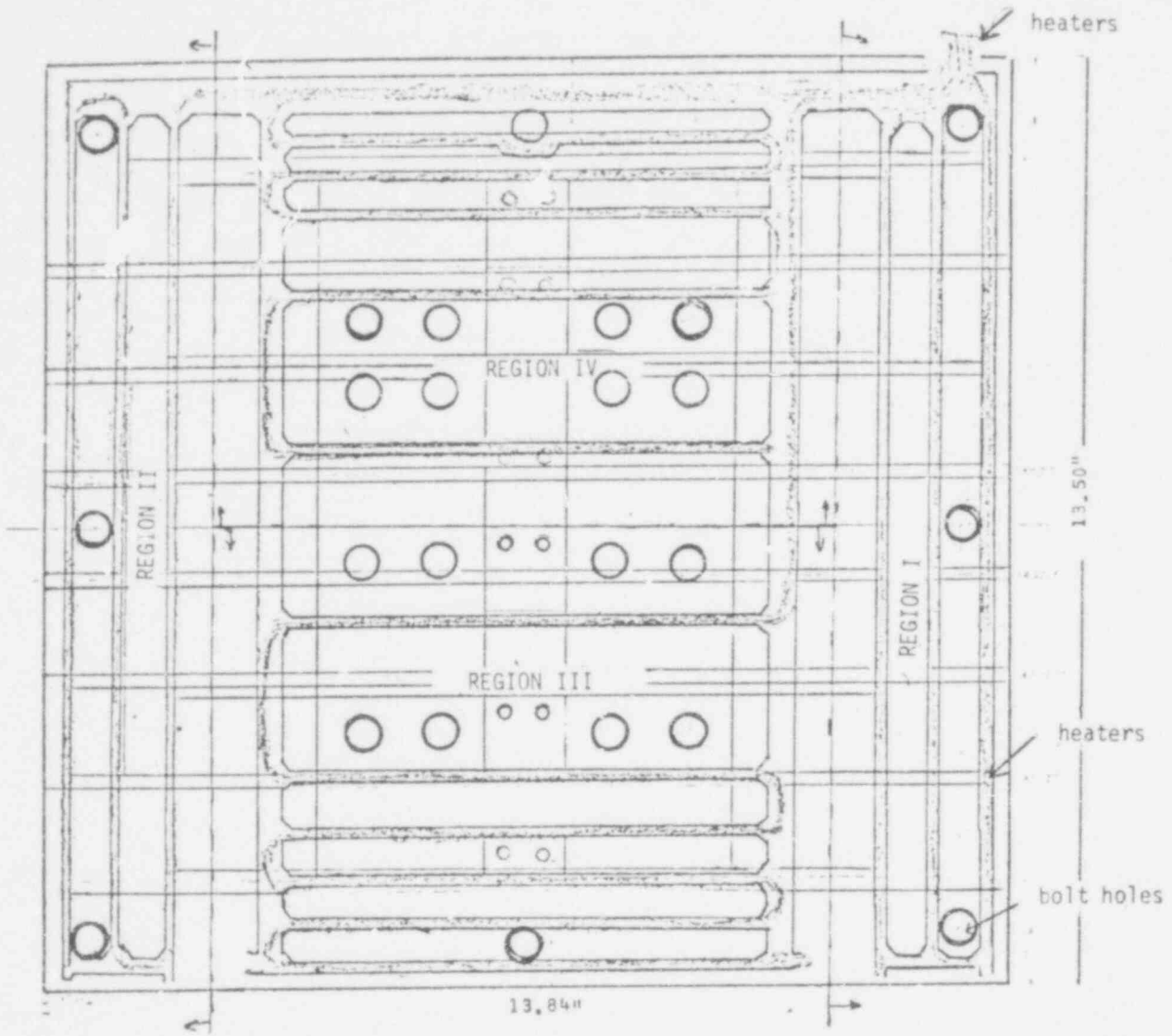

FIGURE ORNL-5. Heater Plate Layout of Heated Regions.

Rockwell International Energy Systems Group (RIES)

APPLICATION OF HELIUM ACCUMULATION FLUENCE MONITORS TO LIGHT WATER REACTOR SURVEILLANCE

B. M. Oliver and Harry Farrar IV

Objectives

1. Apply helium accumulation fluence monitors (HAFM's) to the surveillance dosimetry of light water reactor systems.

2. Fabricate and test selected sets of HAFM's in LWR and benchmark neutron environments.

3. Examine the feasibility of using helium buildup in pressure vessel materials as a surveillance monitoring procedure.

4. Formulate ASTM recommended practices and procedures for HAFM's in light water reactor systems.

Summary

Helium analyses have been completed on the boron and lithium HAFM's irradiated in the Fission Cavity of the BR1 reactor at Mol, Belgium. Preliminary results of these analyses are reported here. These results have not yet, however, been corrected for such factors as neutron self-shielding and flux gradients.

A total of 113 HAFM's have been fabricated and shipped to CEN/SCK for inclusion in the cooperative LWR-PV steels test irradiation in the FRJ-1 and FRJ-2 reactors in Jülich, West Germany. The HAFM's will be irradiated in both core and reflector locations, and the results will be compared with data from HEDL and CEN/SCK dosimeters irradiated at the same locations.

Accomplishments and Status

I. Helium Analysis of ^{10}B and ^{6}LiF HAFM's in the BR1 Fission Cavity

During the report period, helium concentration measurements have been completed on the 24 natural boron bare crystals, enriched ^{6}LiF (99.1% ^{6}Li) bare crystals, enriched ^{10}B (93.0% ^{10}B) HAFM capsules, and enriched ^{6}LiF HAFM capsules irradiated in the Fission Cavity of the BR1 reactor at CEN/SCK in Mol, Belgium. Funding for ten of these helium analyses (HAFM capsules) is being provided by a HEDL contract, as part of the LWR Pressure Vessel Irradiation Surveillance Dosimetry Program. This irradiation was conducted concurrently with a similar irradiation of boron and lithium HAFM's in the Sigma Sigma benchmark neutron field of the BR1 reactor. Both irradiations, conducted in cooperation with other laboratories participating in the Interlaboratory Reaction Rate (ILRR) program, are an integral part of Rockwell International's overall program to demonstrate and develop the use of HAFM's for neutron dosimetry. The purpose of the irradiation was to measure the helium production cross section of ^{10}B and ^{6}Li in the ^{235}U fission neutron spectrum. Preliminary results from approximately one-half of the samples were given in the previous quarterly report.[1]

Preliminary results of the Fission Cavity helium analyses indicate average ^{4}He concentrations of 0.220 ± 0.006 and 0.198 ± 0.009 atomic parts per billion (appb) for ^{10}B and ^{6}Li, respectively. This gives a ^{10}B-to-^{6}Li reaction ratio of 1.11 ± 0.06, which is somewhat higher than the ~1.0 value obtained using ENDF/B cross section data, assuming a Maxwellian ^{235}U fission neutron spectrum. These results have not yet, however, been adjusted for small correction factors such as neutron self-shielding and flux gradients. Additionally, only a preliminary correction has been made for epithermal wall return background neutrons, which contribute ~10% to the total helium production. This contribution was measured by including additional HAFM's at two other locations in the cavity away from the fission source. A detailed description of the Fission Cavity irradiation, and complete results of the helium analyses are being reported in DOE periodic[2-4] and ILRR program reports, where other related benchmark irradiation experiments are also discussed.

II. FRJ-1 and FRJ-2 Dosimetry Experiment

A total of 113 HAFM's have been prepared and shipped to CEN/SCK for inclusion in the cooperative LWR-PV steels test irradiations in the FRJ-1 and FRJ-2 reactors in Jülich, West Germany. Three separate irradiations are to be conducted starting in September 1978, one in a core location of FRJ-1 and one each in a core location and a reflector location in FRJ-2. The core location exposures will be approximately 10 days, and the reflector exposure approximately 100 days in order to achieve a target neutron fluence (>1 MeV) in each location of 2×10^{19} cm^{-2}. The Rockwell HAFM's are to be included with HEDL dosimetry sets in six small cylindrical argon-filled stainless steel subcapsules. The inside dimensions of these subcapsules are ~0.24 in. ID and ~0.51 in. length. The subcapsules are to be filled with argon to improve thermal conductivity. At CEN/SCK, these subcapsules will be combined with gradient foils and two similar subcapsules provided by CEN/SCK and KFA in a larger gadolinium sheathed stainless steel dosimetry capsule. Two such dosimetry capsules will be irradiated in each of the three irradiation locations.

A complete list of the various elements and compounds included in each Rockwell dosimetry set is given in Table RIFS-1. In total, there are 59 vanadium HAFM capsules, 45 unencapsulated HAFM wire segments, 3 unencapsulated zirconium chunks, and 6 empty vanadium capsules. The elements and compounds in each set include those outlined by HEDL in the irradiation proposal; specifically, wires of Cu, Fe, Ni and alloys containing very low concentrations of ^{10}B and ^{6}Li. The Cu, Fe and Ni have threshold (n,α) reactions and will measure neutron fluences for energies $\gtrsim$3 MeV. The alloys of ^{10}B and ^{6}Li will monitor neutron fluences for energies <1 MeV. The boron and lithium alloys were also included in encapsulated form in order to determine any possible helium loss from either α-recoil or from diffusion.

In addition to these elements and alloys, compounds containing nitrogen (TiN and ZrN) and sulfur (PbS and Cu_2S), and individual samples of beryllium, are also included in each dosimetry set. The (n,α) cross sections of these elements are sensitive to neutron fluences in the 1-3 MeV range and have been proposed by HEDL as potential future LWR-PV surveillance sensors. Unencapsulated

samples of Ti and Zr were included to monitor the background contributions of these elements to HAFM's containing these elements as compound components.

Some additional HAFM's compounds have been included containing fluorine (FeF_2 and CaF_2), oxygen (V_2O_5), chlorine and potassium (KCl). These elements, which have various threshold (n,α) reactions in the range of 2-4 MeV, are currently in the scoping phase as possible LWR dosimeters. Additionally, wire segments of Nb and Pt have been included to measure their background helium production in order to determine their potential value as possible encapsulating materials in future LWR irradiations.

Expected Accomplishments in Next Reporting Period

1. Specify and order homogeneous wire containing low levels of ^{10}B and ^{6}Li.

References

1. B. M. Oliver, Harry Farrar IV, D. W. Kneff, and J. G. Bradley, "Application of Helium Accumulation Fluence Monitors to Light Water Reactor Surveillance," LWR Pressure Vessel Irradiation Surveillance Dosimetry Quarterly Report, January-March 1978, NUREG/CR 0285, HEDL-TME 78-6, Hanford Engineering Development Laboratory, Richland, WA.

2. H. Farrar IV, J. G. Bradley and B. M. Oliver, Technical Progress Report - Fast Reactor Fluence Dosimetry, June-December 1977, AI-DOE-13209, Atomics International, March 1978.

3. H. FARRAR IV, J. G. Bradley and B. M. Oliver, Technical Progress Report - Fast Reactor Fluence Dosimetry, January-March 1978, AI-DOE-13236, Atomics International, May 1978.

4. B. M. Oliver, J. G. Bradley and H. Farrar IV, Semiannual Technical Progress Report - Fast Reactor Fluence Dosimetry, April-September 1978, ESG-DOE-13260, Rockwell International, Energy Systems Group, December 1978.

TABLE RIES-1

HELIUM ACCUMULATION MATERIALS AND SUGGESTED
LOADING PRIORITY FOR FRJ-1 AND FRJ-2 IRRADIATIONS

Sample Description	Dimension (inch)	Loading Priority	Number of Samples in Each Dosimetry Capsule					
			FRJ-1 Core		FRJ-2 Core		FRJ-2 Reflector	
			No. 1	No. 2	No. 1	No. 2	No. 1	No. 2
Fe Wire	0.040 x 0.5	1	1	1	1	1	1	1
Ni Wire	0.040 x 0.5	2	1	1	1	1	1	1
Cu Wire	0.030 x 0.5	3	1	1	1	1	1	1
Al Wire	0.040 x 0.5	4	1	1	1	1	1	1
Ni-0.13% ^{10}B Wire	~0.05 x 0.25	5	1	1	1	1	1	1
Al-0.6% ^{6}Li Wire	~0.05 x 0.25	6	1	1	1	1	1	1
Ti Wire	0.020 x 0.5	10	1	0	1	0	1	0
Nb Wire	0.020 x 0.5	16	1	0	1	0	1	0
Pt Wire	0.021 x 0.5	17	1	0	1	0	1	0
Ni-0.13% ^{10}B Wire	Vanadium Encapsulated 0.050 x 0.25	7	1	0	1	0	1	0
Al-0.6% ^{6}Li Wire		8	1	0	1	0	1	0
Blank		9	1	1	1	1	1	1
TiN Powder		10	1	1	1	1	1	1
PbS Powder		11	1	1	1	1	1	1
Be Crystal		12	2	1	2	1	2	1
ZrN Powder (Lot A)		13	1	1	1	1	1	1
Cu_2S Powder		14	1	1	1	1	1	1
ZrN Powder (Lot B)		15	1	1	1	1	1	1
FeF_2 Powder		18	0	0	2	0	2	0
V_2O_5 Powder		19	0	0	1	0	1	0
CaF_2 Powder		20	0	0	2	0	2	0
KCl Powder		21	0	0	2	0	2	0
Zr Chunks	~3-8 mg	13	1	0	1	0	1	0
		Totals	20	13	27	13	27	13

Total Number of Samples; 113.

DISTRIBUTION

R5 (375)

U.S. DEPARTMENT OF ENERGY (4)
FFTF Project Office
P.O. Box 550
Richland, WA 99352
- A. R. DeGrazia
- T. King

Reactor Research & Technology
Department of Energy
Washington, D.C. 20545
- Chief, Reactor Physics Branch
- J. W. Lewellen

AERE HARWELL (2)
Oxfordshire OX11 ORA
UNITED KINGDOM
- L. M. Davies
- A. J. Fudge

AERE WINFRITH (4)
Dorchestor, Dorset
UNITED KINGDOM
- J. Butler
- C. G. Campbell
- A. K. McCracken
- J. Sanders

ARGONNE NATIONAL LABORATORY (1)
9700 South Cass Avenue
Argonne, Il 60439
- Roland J. Armani
  Building 316

BABCOCK & WILCOX (1)
Lynchburg Research Center
Post Office Box 1260
Lynchburg, VA 24505
- R. H. Lewis

515 272

DISTRIBUTION (cont'd)

BATTELLE-COLUMBUS (2)
505 King Avenue
Columbus, OH 43201
- D. Farmelo
- J. Perrin

BROOKHAVEN NATIONAL LABORATORY (3)
National Neutron Cross Section Center
Upton, N.Y. 11973
- J. F. Carew
- B. A. Magurno
- Sol Pearlstein, Building T-197

CENTRE D'ETUDES NUCLEAIRES de SACLAY (3)
B. P. No. 2
91190 Gif sur Yvette
FRANCE
- A. A. Alberman
- J. M. Cerles
- J.P. Genthon

CENTRE D'ETUDE de l'ENERGIE NUCLEAIRE (4)
Boeretang 200
Mol, Belgium
- J. Debrue
- G. DeLeeuw
- S. DeLeeuw
- Albert Fabry

COMBUSTION ENGINEERING (1)
1000 Prospect Hill Road
Windsor, Connecticut 06095
- J. Varsik

COMMONWEALTH EDISON (1)
P.O. Box 767
Chicago, IL 60690
- A. D. Rossin

EG&G IDAHO, INCORPORATED (3)
P.O. Box 1625
Idaho Falls, ID 83401
- R. Greenwood
- Y. Harker
- J. W. Rogers

515 273

ELECTRIC POWER RESEARCH INSTITUTE (5)
3412 Hillview Avenue
P.O. Box 10412
Palo Alto, CA 94304
- T. Marston
- O. Ozer
- F. J. Rahn
- K. Stahlkopf
- H. A. Till

EURATOM (3)
JRC Ispra
I 21020 Ispra (VA)
ITALY
- R. Dierckx

Comitato Nazionale Per L'Energie Nucleare
Centro Di Studi Nucleari Della Casaccia
Casella Postale 2400
00060 Santa Maria di Galeria
Rome, Italy
- Dr. Ugo Farinelli

ECN Netherlands Energy Research Foundation
Weterduinweg 3
Petten, (N.H.)
NETHERLANDS
- W. L. Zijp

FRACTURE CONTROL CORPORATION (1)
330 South Kellogg Avenue
Suite E
Goleta, CA 93017
- Richard A. Wullaert

GENERAL ELECTRIC COMPANY (1)
Vallecitos Nuclear Center
Post Office Drawer B
Vallecitos Road
Pleasanton, CA 94566
- Gerald C. Martin

515 274

DISTRIBUTION (cont'd)

INTERNATIONAL ATOMIC ENERGY AGENCY (2)
Karntner Ring 11
Post Office Box 590
A-1011 Vienna
AUSTRIA
- V. Chernyshev
- J. Schmidt

IKE - STUTTGART (1)
Postfach 801140
7000 Stuttgart-80 (Vaihingen)
PFAFFENWALDRING 31
WEST GERMANY
- G. Prillinger

IRT CORPORATION (3)
P. Box 80817
San Diego, CA 92183
- N. A. Lurie
- C. Preskitt
- W. E Selph

KFA - ZBB
Kernforschungsanlage Jülich Gmbh (2)
Postfach 1913
D-5170 Julich 1
WEST GERMANY
- D. Pachur
- W. Schneider

LOS ALAMOS SCIENTIFIC LABORATORY (2)
University of California
P.O. Box 1663
Los Alamos, NM 87544
- Gordon Hansen, Group N-2
- L. Stewart

MACALESTER COLLEGE (1)
Dept. of Physics & Astronomy
St. Paul, MN 55105
- J. H. Roberts

515 275

DISTRIBUTION (cont'd)

NATIONAL BUREAU OF STANDARDS (4)
Center of Radiation Research
U.S. Department of Commerce
Washington, D.C. 20234
- R. S. Caswell
- C. M. Eisenhauer
- J. A. Grundl
- E. D. McGarry

NAVAL RESEARCH LABORATORY (3)
Thermostructural Materials Branch
Code 6392
Engineering Materials Division
Washington, D.C. 20375
- R. Hawthorne
- L. Steele
- M. Rosen
Code 6653

NUCLEAR REGULATORY COMMISSION (9)
Metallurgy & Materials Research Branch
Mail Stop SS-1130
Washington, D.C. 20555
- Chief
- Public Document Room (3)
- R. Gamble
- K. G. Hoge
- W. Morris
- P. N. Randall
- C. Z. Serpan
- S. H. Weiss

OAK RIDGE NATIONAL LABORATORY (12)
P.O. Box Y
Oak Ridge, TN 37830
- R. G. Berggren
- J. A. Conlin
- S. S. Hurt
- F. B. K. Kam
- R. E. Maerker
- L. F. Miller
- F. R. Mynatt
- F. Perey
- I. Siman-Tov
- F. W. Stallmann
- J. H. Swanks
- C. R. Weisbin

515 276

ORTEC, INC. (1)
100 Midland Road
Oak Ridge, TN 37830
- W. Zimmer

PACIFIC NORTHWEST LABORATORY (2)
- William C. Morgan
Materials Department
PSL Building/Room 1303
Richland, WA 99352

- Clarence A. Oster
Engineering Physics Department
Math Building/Room 1248
Richland, WA 99352

RADIATION RESEARCH ASSOCIATES (2)
3550 Hulen Street
Ft. Worth, TX 76107
- R. M. Rubin
- M. B. Wells

ROCKWELL INTERNATIONAL ENERGY SYSTEMS GROUP (2)
P.O. Box 309
Canoga Park, CA 91304
- Harry A. Farrar IV
- Brian Oliver

ROLLS-ROYCE & ASSOCIATES LIMITED (2)
P. O. Box No. 31
Derby, England
- M. Austin
- P. Burch

SCIENTIFIC APPLICATIONS INCORPORATED (3)
1200 Prospect Street
LaJolla, CA 92037
- W. Hagan
- L. Simmons
- V. V. Verbinski

SOUTHWEST RESEARCH INSTITUTE (1)
8500 Culebra Road
Post Office Box 28510
San Antonio, TX 78284
- E. B. Norris

515 277

UNIVERSITY OF CALIFORNIA SANTA BARBARA (1)
Department of Chemical & Nuclear Engineering
Santa Barbara, CA 93106
- G. Robert Odette

UNIVERSITY OF TOKYO (2)
Dept. of Nuclear Engineering
7-3-1, Hongo
Bunkyo-ku, Tokyo
JAPAN
- M. Nahazawa
- J. Sekiguchi

WESTINGHOUSE ELECTRIC CORPORATION (8)
Advanced Nuclear Systems Division
P.O. Box 355
Pittsburgh, PA 15230
- G. W. Hardigg, General Manager

Light Water Power Division
P.O. Box 355
Pittsburgh, PA 15230
- S. Anderson
- J. Davison
- T. R. Mager
- J. J. Taylor
- S. E. Yanichko

Research Division
P.O. Box 355
Pittsburgh, PA 15230
- R. Holland
- J. A. Spitznagel

HANFORD ENGINEERING DEVELOPMENT LABORATORY (27)
P.O. Box 1970
Richland, WA 99352

- H. J. Anderson W/A 40
- R. A. Bennett W/F121B
- F. M. Berting W/A-57
- T. K. Bierlein W/A-57
- W. L. Bunch W/F121B
- L. L. Carter W/F121B
- T. Chiao W/A-39
- C. K. Day W/A-56

515 278

DISTRIBUTION (cont'd)

- D. G. Doran W/A 57
- E. A. Evans W/C 16
- R. Gold W/A 39
- G. L. Guthrie W/A 39
- G. J. Holmes W/A 58
- L. A. James W/A-40
- B. J. Kaiser W/A-56
- L. S. Kellogg W/A 37
- R. L. Knecht W/A 40
- J. J. Laidler W/A 57
- E. F. Lippincott W/A 39
- W. Y. Matsumoto W/A 33
- W. N. McElroy W/A 39
- P. A. Ombrellaro W/F121B
- L. M. Osland W/C 115
- R. E. Peterson W/F 109
- F. H. Ruddy W/A-39
- R. E. Schenter W/F 429
- F. A. Schmittroth W/F121B
- E. M. Sheen W/A-56
- F. R. Shober W/E-6
- R. L. Simons W/A 57
- J. A. Williams W/A 40
- J. G. Wise W/A 21
- J. B. Yasinsky W/B 65
- H. H. Yoshikawa W/A 62
- Central Files (2)
- Program Files, (5)

c/o W. N. McElroy W/A 39

515 279

NRC FORM 335 (7.77)

U.S. NUCLEAR REGULATORY COMMISSION

BIBLIOGRAPHIC DATA SHEET

1. REPORT NUMBER (Assigned by DDC)
NUREG/CR-0550

4. TITLE AND SUBTITLE (Add Volume No., if appropriate)
LWR Pressure Vessel Irradiation Surveillance Dosimetry, Quarterly Progress Report, April-June 1978

2. (Leave blank)

3. RECIPIENT'S ACCESSION NO.

7. AUTHOR(S) G.L. Gutherie, W.N. McElroy, E.P. Lippincott

5. DATE REPORT COMPLETED
MONTH April YEAR 1979

9. PERFORMING ORGANIZATION NAME AND MAILING ADDRESS (Include Zip Code)
Hanford Engineering Development Lab
P.O. Box 1970
Richland, WA 99352

DATE REPORT ISSUED
MONTH June YEAR 1979

6. (Leave blank)

8. (Leave blank)

12. SPONSORING ORGANIZATION NAME AND MAILING ADDRESS (Include Zip Code)
Office of Nuclear Regulatory Research
U.S. Nuclear Regulatory Commission
Washington, D. C. 20555

10. PROJECT/TASK/WORK UNIT NO.

11. CONTRACT NO.
NRC FIN No. B5988-7

13. TYPE OF REPORT
Quarterly Progress Report

PERIOD COVERED (Inclusive dates)
April - June 1978

15. SUPPLEMENTARY NOTES

14. (Leave blank)

16. ABSTRACT (200 words or less)

This report describes progress made in the Light Water Reactor Pressure Vessel Irradiation Surveillance Dosimetry Program during the reporting period.

The primary objective of the multi-laboratory program is to prepare an updated and improved set of dosimetry, damage correlation, and associated reactor analysis ASTM Standards for LWR-PV irradiation surveillance programs. Supporting this objective are a series of analytical and experimental validation and calibration studies in "Standard, Reference, and Controlled Environment Benchmark Fields," reactor "Test Regions," and operating power reactor "Surveillance Positions."

17. KEY WORDS AND DOCUMENT ANALYSIS

17a. DESCRIPTORS

515 280

17b. IDENTIFIERS/OPEN-ENDED TERMS

18. AVAILABILITY STATEMENT
Unlimited

19. SECURITY CLASS (This report)
Unclassified

21. NO. OF PAGES

20. SECURITY CLASS (This page)

22. PRICE
$

515 281